SYNTHESIS, CHARACTERIZATION AND TRIBOLOGICAL PROPERTIES OF Mo-DLC

By

TIRTH ASHISHBHAI PATEL

Presented to the Faculty of the Graduate School of

The University of Texas at Arlington in Partial Fulfillment of

the requirement for

the degree of

MASTER OF SCIENCE IN MATERIALS SCIENCE AND ENGINEERING

THE UNIVERSITY OF TEXAS AT ARLINGTON

December 2021

ACKNOWLEDGEMENTS

I would like to express my sincere gratitude to my research advisor, Dr. Efstathios I. Meletis for his constant guidance and encouragement throughout the research. I am thankful to Dr. Pranesh Aswath, Dr. Jiechao Jiang and Dr. Ye Cao for their time and participation as my defense committee members as well for as their suggestions.

I am thankful to Dr. Yi Shen and Chuzhong Zhang for their guidance and help during characterization. I would like to thank my colleagues Ignacio Lopez Cabanas, Hunter Pitts, Theofilos Karavasilis, Dr. Wisanu Boonrawd, Dr. Hooman Rahmani, Christiniece Pope for their moral support and enduring help during research work. I am also thankful to directors and operational personals of various labs at UTA which helped in my research, Surface and Nano Engineering Lab (SaNEL), Characterization Center for Materials and Biology.

At the end I would like to thank my parents and family for their constant support and belief in me. I wouldn't have achieved this without them.

December 6, 2021

ABSTRACT

SYNTHESIS, CHARACTERIZATION AND

TRIBOLOGICAL PROPERTIES OF Mo-DLC

Publication No._____

Tirth Ashishbhai Patel; M.S.

The University of Texas at Arlington, 2021

Supervising Professor: Dr. Efstathios I. Meletis

Diamond like carbon (DLC) films have been extensively used in a wide range of applications over the last decade due to their excellent mechanical and tribological properties. Metallic elements are used to dope DLC films in an effort to overcome some DLC limitations and make it compatible to use it in larger variety of applications. This study focuses on the effect of different processing parameters on DLC deposition, and the effect of Mo content on microstructure, mechanical and tribological properties. Plasma Enhanced Chemical Vapor Deposition (PECVD) technique coupled with magnetron sputtering is used in chamber atmosphere composed of CH_4 and Ar to synthesize DLC films with various Mo content. Mo-DLC films were deposited using pulsed DC bias on substrate with DC power on target, and DC bias on substrate with pulsed DC power on

target. These DLC and Mo-DLC films were characterized by optical profilometer, Scanning Electron Microscopy (SEM), Electron Dispersive Spectroscopy (EDS), Atomic Force Microscopy (AFM), Transmission Electron Microscopy (TEM), X-Ray Diffraction (XRD), and Raman spectroscopy. Nano-indentation tests were carried out to assess the hardness of the Mo-DLC films. Tribological tests were conducted with and without oil to study the steady state Coefficient of Friction (COF) and wear rate of DLC and Mo-DLC films as a function of Mo content.

Film thickness, topography, and Mo content results from profilometry, and SEM/EDS study revealed that only deposition rate is affected by target power type, and neither surface finish nor Mo content are affected. The maximum deposition rate of 33 nm/min and 27 nm/min were achieved for pulsed DC power and DC power on the Mo target, respectively. Residual stress measurements showed a significant reduction with increasing Mo content from 1.5 GPa in pure DLC to 0.3 GPa for 16.9 at.% Mo-DLC. AFM measurements showed very smooth film surfaces with roughness values around 14 nm and 17 nm for 4.2 at.% Mo and 11.8 at.% Mo, respectively. TEM observation and SAD pattern analysis revealed that Mo is present as nano particles that were distributed uniformly in amorphous DLC matrix forming a cubic MoC phase. With increase in Mo content from 4.2 at.% to 11.8 at.% the MoC grain size increased from 2.20 nm to 3.10 nm while the MoC clusters remained surrounded by graphitic boundaries. Diffraction peak position and FWHM of peaks from XRD study also confirmed the formation of cubic MoC with grain size 2.89 nm and 3.05 nm for 7.5 at.% Mo and 11.8 at.% Mo, respectively. The Raman spectra revealed that sp^2 content in DLC film increases with increase in Mo content. With doping 4.2 at.% Mo in DLC, hardness decreases from 14.20 GPa to 12.60 GPa which remains almost the same with further increase in Mo content. The lowest steady state COF of Mo-DLC films for dry sliding was 0.115 while that for DLC was 0.1. The lowest specific wear rate in dry sliding it was observed for 6 at.%

Mo-DLC ($24*10^{-8}$ mm^3/N-m) that compared well with that of pure DLC ($7*10^{-8}$ mm^3/N-m). This behavior is consistent with higher sp^2 content resulting from Mo doping. In oil lubricated sliding, low COF were observed for both Mo-DLC and DLC (0.065 and 0.085, respectively) with no signs of wear even after testing for 3000 m sliding distance.

TABLE OF CONTENTS

LIST OF ILLUSTRATIONS

List of Tables

CHAPTER 1

INTRODUCTION

Carbon is available in various forms in environment which includes its forms of diamond and graphite. Carbon in diamond is arranged in the network structure of sp^3 domains. Diamond is considered as a unique material due to properties like high hardness, low wear rate, thermal conductivity, optical transparency, and chemical inertness. But because of high coefficient of friction (COF), its applications are limited. On the other hand, graphite has carbon arranged in network structure of sp^2 domains. Each carbon atom is connected to three different carbon atoms in the same plane leaving one electron free to migrate. These layers are connected to each other with weak van der Wall's forces, which makes them slid past each other easily [1]. Graphite has very low friction coefficient and good thermal conductivity but with limitation of low hardness and high wear rate. Diamond-like carbon (DLC) is developed to have properties of both diamond and graphite with carbon in both sp^2 and sp^3 bonds. The state of carbon in the film is mainly amorphous with coexistence of small clusters of microcrystalline structure [2]. It is also known as hydrogenated amorphous carbon (a-C:H) or amorphous carbon (a-C). DLC has become major research area after Aisenberg and Chabot's report in 1971 due to their potential as advanced solid lubricant coatings [3].

DLC films have high hardness, high thermal conductivity, low wear rate, low friction coefficient, good chemical stability, good bio compatibility. Which leads to its use in bio implants, engine parts and corrosion resistant parts. Very low friction coefficient of 0.05~0.06 has been reached without any external lubrication [4, 5]. The low friction coefficient and low wear rate of

DLC is related to formation and transfer of a graphitic layer of critical thickness and, presence of low-strength atomic carbon interlayer in the produced graphite like structure [4]. These properties make it usable for many applications.

Over the time tribological properties of DLC have been studied and it has come to light that it is highly unstable at higher temperature. At temperature above 350°C graphitization takes place, which further reduces the friction coefficient but at cost of high wear rate. In addition to that, DLC has low toughness and adhesion on metal substrate. At normal room temperature, graphitization is induced due to wear during sliding motion. There is requirement of graphitization for formation of transfer layer, but it should be in limit to avoid high wear rate [3, 5, 6]. Also, toughness of DLC films is low [7].

In addition to low toughness and instability at high temperatures, one other limiting factor is thickness of film. It tends to delaminate from the substrate due to residual stresses, which increase with thickness [8]. The high compressive residual stresses originate from the formation of sp^3 interatomic bonding, which is related to the diamond phase of the film. These stresses further increase due to bombardment of high energy ions during deposition, and temperature changes. High residual stress leads to different failure modes like telephone cord blister, circular blister, interface delamination, cracking, channeling etc. These failure modes can take place even before the film has been put in to use. By reducing the residual stresses in the film, adhesion can be improved, and the above listed failures can be prevented.

One way to reduce the residual stress is to incorporate metal atoms in DLC during deposition. This dopes film is also known as “Me-DLC”. By incorporation of metal atoms, some sp^3 carbon-carbon bonds will be replaced with carbon-metal bonds. Interatomic forces in these bonds are weaker than sp^3 C-C bonds, lowering the residual stress and hardness as well. With

increase in metal content in DLC, ductility also increases. Incorporation of Mo in DLC can behave better than incorporation of other metals like Ag, Cu and W in terms of tribological properties. There have been studies in the area of Mo-DLC which show excellent tribological properties at high temperature (400°C and 500°C) and room temperature, which proves its stability at higher temperatures [9, 10]. As Mo and DLC both are bio-compatible materials, it's application in bio-implants has been explored as well [9]. Mo-W-C films have shown promising tribological properties with very low COF of 0.07 with oil lubrication. The COF is result of formation of lubricious MoS_2 by reaction of S from oil with Mo of film [11, 12]. Mo-DLC film has been studied over the time for its properties, but these studies lack an explanation of microstructural changes over different Mo content, effect of different deposition parameters on film properties and tribological properties in presence of oil lubrication.

The present research focuses on the study of the effect of deposition parameters, microstructure , friction coefficient and wear rate in dry and lubricated sliding conditions for Mo-DLC as a function of Mo content. Mo-DLC thin films were deposited on Si_{100} wafer using two different combination of power supply, varying working pressure, and the CH_4 content in the gas flow. Films were characterized with Scanning Electron Microscopy (SEM), X-Ray Diffraction (XRD), Raman spectroscopy and Transmission Electron Microscopy (TEM). Hardness and elastic modulus of films were determined using nano-indentation. Tribological properties were studied using pin-on-disk test geometry with and without lubrication. Chemical composition and surface morphology of wear tracks and wear pin were investigated with optical profilometer and SEM-EDS.

CHAPTER 2

OBJECTIVE

In the present research work, diamond like carbon is doped with Mo with prospective of use at high temperature in engine parts like piston rings and valves. Plasma Enhanced Chemical Vapor Deposition (PECVD) coupled with magnetron sputtering is used for the deposition of Mo-DLC. The Objectives of this work were to study:

- Effect of processing parameters on the structure and properties of Mo-DLC
- Effect of pulsed DC and DC power supply on deposition rate and film characteristics
- Microstructure and properties evolution over the range of Mo content in Mo-DLC films
- Frictional and wear behavior of Mo-DLC films

CHAPTER 3

LITERATURE REVIEW

3.1 Diamond-like Carbon Thin Films

Aisenberg and Chabot were the first to successfully synthesize DLC with Ion beam deposition technique [13]. Over the time, new techniques were developed to deposit thin films. All the deposition methods can be divided in to two categories namely, Physical Vapor Deposition (PVD) and CVD. PVD involves vaporizing target material and deposition of that vapor on to the substrate. In this case carbon target is used. On the other hand, gas containing carbon such as CH_4 and C_2H_2 is used for source of carbon. PVD and CVD for DLC deposition can be further classified as below.

(a) Ion beam deposition

(b) Cathodic arc deposition

(c) Pulsed laser deposition

(d) Magnetron sputtering

(e) Plasma enhanced chemical vapor deposition

3.1.1 Deposition methods for DLC

a. Ion-beam deposition

Ion-beam deposition (IBD) method was the first method used for deposition of DLC by Aisenberg and Chabot. In this method, an ion source is used to ionize the carbon atoms from the gas or target. In typical IBD system, carbon ions are produced from plasma sputtering of carbon target by ion source. A voltage bias is applied on the substrate holder to attract these ions from the plasma. These attracted carbon ions get deposited on the substrate creating a very thin layer of

carbon atoms which is called DLC. In place of carbon target, sometimes CH_4 is also used as source of carbon. The deposition mechanism remains the same for that as well [13, 14]. In this technique medium energy carbon or hydrocarbon ions (~100 eV) will be condensed to form DLC.

There exists a slight modification in this technique named as mass selected ion beam (MSIB) in which controlled deposition is accomplished from single ion species with controlled ion-energy [15, 17]. Carbon ions are produced from a graphite target with small spread of ion energy around 1-10 V, which are accelerated to 5-40 kV and passed through a magnetic filter. This filter riddles neutrals and selects the C^+ from charge/mass (e / m). After filtration, only C^+ ions are left in the beam which causes divergence of beam due to coulombic forces. Then ions are decelerated and focused on the substrate with electronic lens. This process gives more control over quality of film, with control over species and energy but has very low deposition rate of 0.001 Å/s at high cost and size of apparatus.

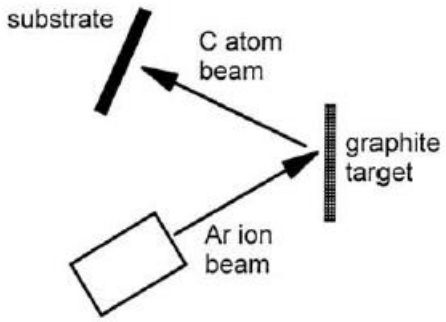

Figure 1: Ion beam deposition

b. Cathodic arc deposition

When a small carbon striker electrode is touched and withdrawn from a graphite cathode, an arc is generated. This leads to formation of plasma with high ion density of 10^{13} ions/cm^3. A low voltage, high current power supply is being used for this purpose. The cathode spot is small

which is formed by an explosive emission process. Plasma as well as particulates are formed due to this process, which are filtered with toroidal magnetic filter generating 0.1 T magnetic field. The electrons from plasma spirals around this magnetic field along the filter axis, which creates electrostatic field, causing positive ions from plasma to follow electrons around the filter. The particulates from plasma cannot follow the field and hit the walls. This process is called filtered cathodic vacuum arc. This gives faster deposition compared to ion beam deposition at low capital cost. For some application filtration is not good enough and unstable cathode spot [15].

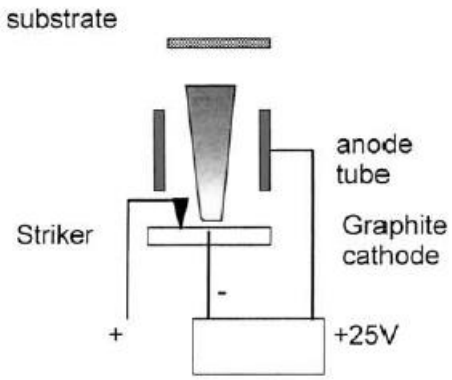

Figure 2: Cathodic arc vacuum deposition

c. Pulsed laser deposition

In this method very short and intense energy pulses are used to vaporize material as an intense plasma [18]. The plasma expands towards the substrate. Due to this expansion, ions have energy nearly like MSIB. Pulsed laser deposition is more versatile compared to MSIB [19].

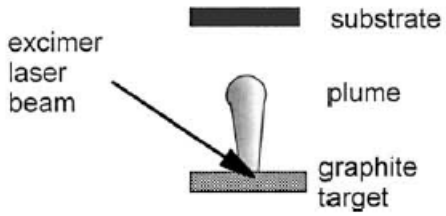

Figure 3: Pulsed laser deposition

d. Sputtering

The most common method used for deposition is sputtering. It uses DC, RF, or pulsed DC sputtering of a graphite target by Ar plasma. High deposition rate is obtainable through this process since graphite has low sputter yield. Figure 4 shows the schematic of magnetron sputtering. A target is attached on top of magnetron gun and when current is passed through the gun, the magnets cause the electron to spiral, which results in longer path length. This causes more degree of ionization in plasma. In some cases, magnetic field can also be configured around the substrate holder to get Ar ions to also bombard the substrate. This configuration is called unbalanced magnetron. DC bias can also be applied to substrate to vary the ion energy. In the above two cases, DLC is deposited from C source. Since there is no H present in the film, the film is going to be ta-C. To get a-C:H, Ar is used as plasma source and hydrocarbon such as CH_4 or graphite target with H_2 gas is introduced into the chamber with bias on substrate. This is called reactive sputtering.

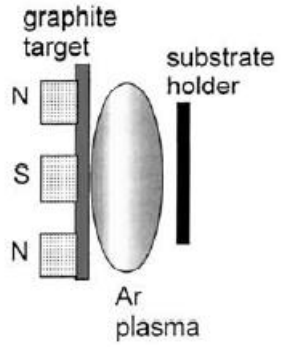

Figure 4: Sputtering

e. PECVD

PECVD uses gases like CH_4 and C_2H_2 as source of carbon and chemical process as the condensing method. In PECVD there are two electrodes, one is cathode, and one is earthed. Cathode is attached to the power supply. Different kind of power supply like DC, RF and pulsed

DC can be used to bias the cathode which serves as substrate holder. Proper dilution ratio is selected for Ar and precursor gases that are allowed to flow into the chamber. Applying power supply produces the plasma between the two electrodes in vacuum. The plasma has net positive charge compared to electrode which leads to attraction towards cathode. This technique is very often used to deposit amorphous hydrogenated DLC. PECVD gives good deposition rate at lower temperature with minimal contamination. The ion energy depends on the voltage bias as well as working pressure of chamber. Since the ion energy controls the sp^3 and sp^2 content, by varying voltage bias and working pressure desired sp^3/sp^2 can be obtained [20, 21].

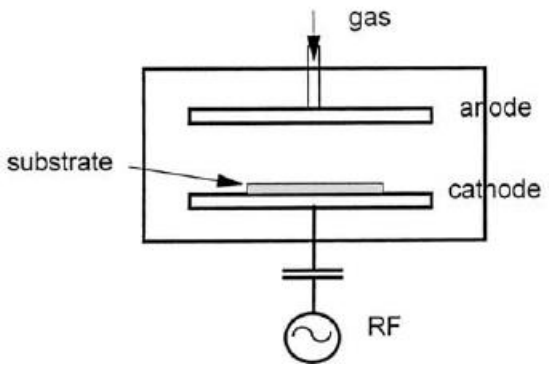

Figure 5: PECVD

3.1.2 Structure and classification

DLC films have become a unique research area due to their properties like good hardness, good biocompatibility, low friction coefficient and wear rate, chemically inertness, thermal conductivity, electrical resistivity, and optical properties. DLC films are widely used in magnetic storage disk, automobile plants, in engine parts of high-speed cars like NASCAR, knee replacement, drills, bearings and many others [22, 23].

It is well known that there are many allotropes of carbon named as graphite, diamond, buckminsterfullerene, nanotubes and more. Carbon forms many crystalline and disordered

structures. Three stable hybridizations exist for carbon named as sp, sp^2, and sp^3. In diamond, each carbon is bonded with other 4 carbons with covalent bonds making sp^3 bonding. It makes tetrahedral molecular structure. Each bond is at an angle of 109.5° with each other. This arrangement gives diamond it's hardness. On the other hand, in graphite each carbon atom is bonded with other 3 carbon atoms with covalent bonding making sp^2 hybridization. All carbon atoms are in the same plane creating a hexagonal structure. Layers of hexagonal structure are stacked up on each other having weak wan der Wall's force. Due to weak forces, these layers can slide very easily on each other which results into low friction coefficient property of graphite. These layers are also known as graphene. The bond length of sp^2 bonds in graphite is shorter than sp^3 bonds of diamond, which means that sp^2 bonds of graphite is stronger than sp^3 bonds of diamond. But arrangement of C atoms in diamond makes it much harder than graphite. Also, C atoms in graphite have one valance electron which contributes toward it's good electric conductive properties.

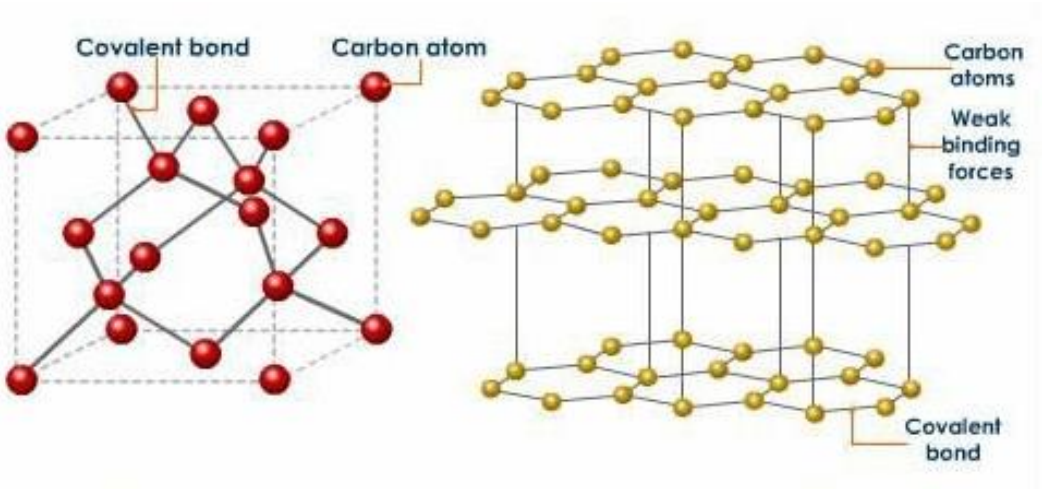

Figure 6: Structure of diamond and graphite

DLC films have a structure of both diamond and graphite. C is found in both sp^2 and sp^3 hybridizations. These films are amorphous since carbon is hybridized in short range order for both

sp^2 and sp^3. Film properties depend on the dominance of sp^2 or sp^3 hybridization. If sp^3 hybridization is dominant in the film, then the film is going to show more diamond like behavior and if sp^2 hybridization is dominant, then the film will show more graphitic behavior. The dominance of sp^3 and sp^2 can be controlled depending on the application by controlling working pressure, applied bias i.e., by controlling ion energy. Figure 7 a is ternary phase diagram of DLC. Robertson [24] mentioned that it was first proposed by Jacob and Moller [25].

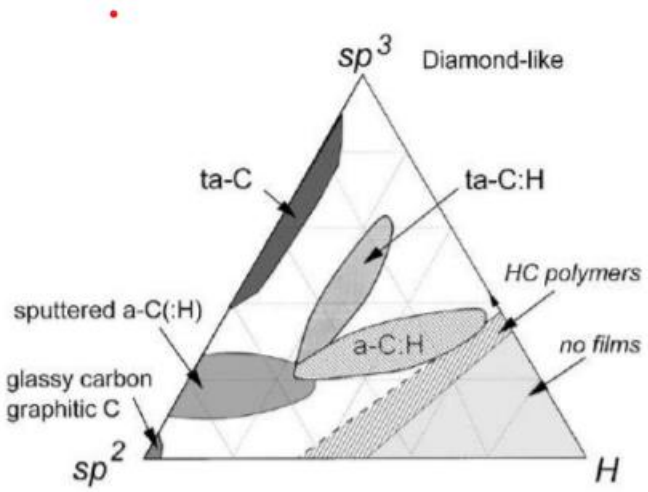

Figure 7: Ternary phase diagram for DLC [26]

At the lower left corner where only sp^2 hybridization exists, the film is glassy carbon and shows mostly graphitic behavior. As the sp^3 hybridization increases, the film shows balanced properties of diamond and graphite at a-C(:H) and ta-C. a-C(:H) is hydrogenated amorphous carbon and ta-C is tetrahedral amorphous carbon. In a-C(:H) sp^3 hybridization is present but sp^2 is still dominant and it has a small amount of hydrogen. In ta-C sp^3 hybridization is dominant over sp^2 and there is no hydrogen present in the film. With the advancement of deposition techniques like PECVD, interior phases of the triangle can be explored. By controlling hydrogen content with sp^2 and sp^3 content, ta-C:H and a-C:H can be obtained. Center zone for a-C:H contains more

hydrogen and low sp^3 bonds than the left zone a-C(:H). The table below shows the general properties of different DLC.

Table 1: Properties of various carbon forms [26]

Material	sp^3 %	Hardness (GPa)	H %	Density (g/cm^3)	Gap (eV)
Diamond	100	100	-	3.5	55
Graphite	0	-	-	2.267	0
a-C (evaporated)	0	3	-	1.9	0.4-0.7
a-C (Sputtered)	5	3	-	2.2	0.5
Ta-C	80-88	80	-	3.1	2.5
a-C(:H) (hard)	40	10-20	30-40	1.6-2.2	1.1-1.7
a-C(:H) (soft)	60	< 10	40-50	1.2-1.6	1.7-4

3.1.3 Mechanical and tribological properties of DLC

a. Hardness

Hardness of DLC film is dependent on the sp^3 hybridization content. High hardness is associated with more sp^3 bonds in the film. The content of sp^3 hybridization can be increased by varying the working pressure and ion energy but after certain level, residual stress in the film is going to affect the film's adhesion to the substrate. Hardness and Young's modulus is measured with nano-indentation. Maximum hardness for amorphous

carbon films is 80 GPa and hydrogenated amorphous carbon is 20 GPa [26]. Hardness is calculated with the equation shown below.

$$H = \frac{P_{\max}}{A_r} \quad (1)$$

where P_{max} is applied maximum load and A_r is the residual indentation area.

b. Residual stress and adhesion

DLC films have been used over the time for various applications because of their adhesive strength. These films have large internal compressive stress which limits the critical thickness to prevent the delamination [27]. This compressive stress is developed because of high energy bombardment of ions at room temperature since atoms lacks mobility at room temperature [27, 54]. An increase in internal stress after the critical limit leads to adhesion failure and delamination. To prevent that, a thin metallic interlayer is typically deposited between the substrate and the DLC film.

c. Friction coefficient

The friction coefficient of DLC films depends on the sp^2, sp^3 bonding and testing conditions like humidity [55]. During the sliding of static partner on the DLC film, bonds of C-H break and film formation of a lubricious tribo-layer takes place which is transferred to the static partner. After that sliding takes place between the film on substrate and film on static partner [4, 50]. At room temperature and low humidity, it gives very low COF. But as humidity increases the transfer layer oxidizes and restricts the formation of contact layer which leads to increased friction coefficient. As per standard practice and ASTM G99-95, a pin material is either SS 440 C or Alumina ball with 95% Al_2O_3. As per the experiments, friction coefficient of DLC remains the same irrespective of static partner material which adds another evidence of the film transfer mechanism [38]. Super low

friction coefficient of 0.01 has been reported in vacuum [56, 57]. In normal room condition, unlubricated condition of film with steel counterpart is like lubricated condition of steel with steel counterpart [15].

d. Wear Rate

When a pin on disc friction test is conducted, material experiences wear. This material loss is measured, and the specific wear rate is calculated. Wear rate of DLC film is as low as 10^{-8} mm^3/N-m. The wear rate changes with metal doping [58].

For very low applied load, elastic contact is there between pin and film, which leaves no wear track. At moderate loads, a permanent groove or wear track is left on the surface and at high load wear track of cracking and deformation is left after testing. So, it is always advisable to check the wear properties in worst condition to get the best out of film. So, film's wear properties should be tested at moderate or higher load.

3.1.4 Application of DLC

a. Automobile and manufacturing industry

DLC has good mechanical properties like high hardness, low friction coefficient, low wear rate, and it has been used in various automotive parts. Because of low wear rate and low COF, it has been used in piston rings of NASCAR, fuel injector parts, valve filter, and gears. It's high hardness and wear resistance makes it usable in wear and abrasive tools like drills and manufacturing machines.

b. Biomedical industry

As DLC has shown excellent chemical stability and bio compatibility, it has been used in bio implants like artificial hip joint. As it has very low wear rate and friction coefficient with good bio compatibility, it is used where bio implants are in contact with other body

parts and have relative motion between them. Figure 8 shows hip joint and artificial hip joint coated with DLC.

(a)

(b)

Figure 8(a) & 8(b) Artificial hip joint [59]

c. Optical devices

Over the time DLC has been used in optical storage device because of their good band gap, transparence, and hardness. It has been proven as good solar photovoltaic material due to semiconducting property of the film [60]. Nitrogen doped DLC has been used as antireflective coating on Si solar cells which leads to improved refractive index and reduced absorption coefficient.

3.2 Metal Doped DLC

In spite of some very good properties of DLC, like low friction coefficient, high hardness, chemical inertness but film has some drawbacks which are listed as following. DLC is deposited with high energy ions bombarded on the substrate. When film formation takes place, due to formation of sp^3 bonds, it creates high compressive stress in the film. This stress is also known as residual stresses. This stress increases with increase in thickness and leads to delimitation of film from substrate. To avoid that, the critical thickness of the film must be limited [27, 28]. Another problem with DLC is its thermal instability at high temperatures. It has been reported by Liu and Meletis that graphitization of DLC takes place around 350°C which converts nearly all sp^3 bonds in to sp^2 bonds [6]. This reduces the friction coefficient of film further but at the expense of very high wear rate. To avoid these limitations, metal is doped in the DLC matrix.

3.2.1 Metal doped DLC composite thin films

As discussed above, metal doping in the film reduces the residual stresses providing good adhesion and stability at higher temperatures. Different elements like Si, N, and metals like Ta, Ti, W, Mo, Cr, Ag, Cu, Ni have been doped in DLC depending on the application of the film. Figure 9 shows the general overview of effect of different doping element. Sometimes more than one metal or element is doped in DLC to get additional advantage [29, 30]. Different metal doped DLC films like Si-DLC, Ag-DLC, Cr-DLC, W-DLC, Mo-DLC, Ti-DLC have been studied over the years for their mechanical properties, structure effect due to doping, bio compatibility, tribology, chemical stability, and high temperature performance [31-47]. DLC and Me-DLC is also studied extensively in SaNEL over the years for their mechanical properties, structural characterization, wear mechanism, bio implant application, and tribology behavior.

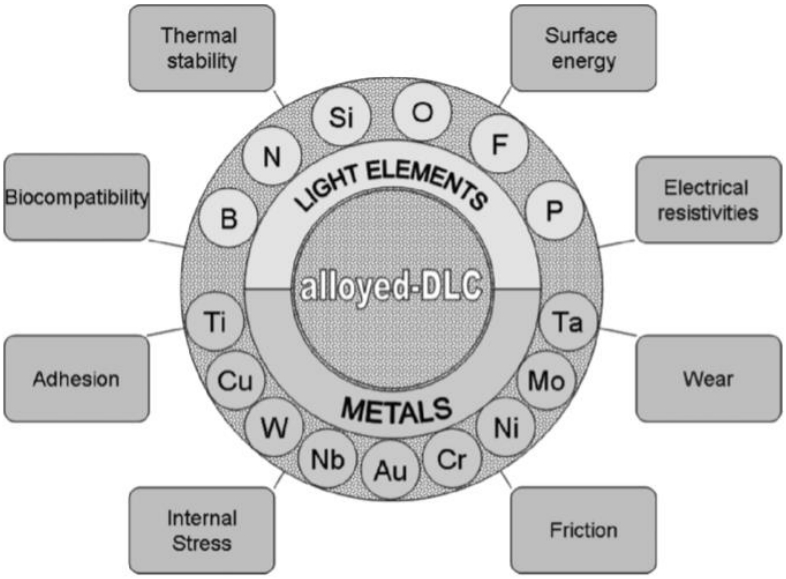

Figure 9: Overview of different doping element on DLC properties [48]

The wear mechanism of DLC and metal doped DLC is the same which involves transfer of a lubricious layer [4, 50]. Metal doped DLC films are generally synthesized using PVD either using one graphite target and one metal target or using a metal target in a hydrocarbon environment with Ar as precursor gas. DLC films with different metal doping like Ti, Mo, W and Nb using PECVD method have been studied by Corbella et al. [51]. Low friction coefficient and wear rate has also been reported with evidence of carbide formation [40, 43, 44, 50].

Co-DLC films were developed for magnetic storage application by CVD/PVD method. Hardness of the films was reduced after metal doping because of decrease in sp^3/sp^2 ratio from 1.3 to 0.87 with increased friction coefficient and wear rate [52]. By doping Cr in DLC, hardness decreases from 16 GPa to 13.5 GPa for 2 at.% of Cr and remains stable up to 18 at.% Cr. CrC was formed which was soluble in DLC matrix up to 1.5 at.% and after that Cr is found in defected CrC nanoparticles at higher Cr content. Cr-DLC has low friction coefficient and wear rate about 10^{-7} $mm^3/N\text{-}m$ up to 12 at.% Cr after that it starts to increase [42]. Ag-DLC was studied over a range of Ag content and 1.3 at.% Ag showed significant reduction in residual stress without significant

effect on film hardness. Friction coefficient increases with increasing Ag content from 0.11 to 0.29. Film with 1.3 at.% Ag had friction coefficient of 0.13 with very low wear rate in the order of 10^{-8} mm^3/N-m [44].

3.2.2 Mo doped DLC thin films

Reports of DLC with several other metals like Ag, Ti, Cr indicate good mechanical and tribological properties. Tang et al. reported that Mo-DLC has shown low friction coefficient at higher temperatures of 400°C and 500°C which proves thermal stability at high temperature as well. They have also shown bone growth and bio compatibility for Mo-DLC [46]. Padmanaban et al. have deposited Mo-DLC using PECVD with pulsed DC sputtering. They have reported friction coefficient of 0.15 for 6.9 at.% Mo at room temperature and surface roughness ranging from 0.7-1.2 nm [48]. Ji et al. reported finding of MoC nano particles implantation in DLC matrix which was beneficial to retain the loss of hardness and elastic modulus [53].

Mo-W-C films have been tested under oil lubrication and without lubrication condition and reported formation of MoS_2 with oil which is a friction reducer tribo-layer [11, 12].

Over the time Mo-DLC has been studied but these studies lack in explanation of the effect of power supply and deposition parameters on Mo content and deposition rate, microstructure evolution over a range of Mo content, wear rate in dry sliding condition, friction coefficient as well as wear rate under oil lubrication conditions.

Chapter 4

EXPERIMENTAL DESIGN AND PROCEDURES

DLC films were synthesized by PECVD with different deposition parameters using Argon and Methane as a precursor gas. The effect of these variables was studied preliminarily and the best condition to deposit DLC was selected. Mo-DLC films were synthesized using the same method coupled with magnetron to vary the Mo content, using different power supplies. The effect of different combinations of power supply was also studied along with the effect of working pressure, and methane content in the total gas glow. The PECVD chamber was designed and build by our research group's previous students. Basic overview of power supply used and PECVD chamber is discussed in next section.

4.1 Synthesis of DLC and Mo-DLC

4.1.1 Hybrid PECVD system coupled with magnetron sputtering

PECVD coupled with magnetron sputtering was used to deposit DLC and Mo-DLC film. The deposition system consists of various power supplies and a vacuum chamber made from stainless steel. A schematic of the chamber inside is shown in Figure 10. The diameter of the cylindrical chamber is 18.38'' and length is 19.66''. There is a co-axial rod with cathode in the middle of it, covered with a shield at bottom part of chamber. Outside the cathode is connected by a universal power supply socket. In the top part of the chamber, there is a magnetron gun of 2'' diameter which can hold targets with thickness 0.125'', 0.185'', and 0.250''. The pneumatic shutter in front of the gun is used to cover the target during plasma cleaning and DLC deposition. The shutter is only opened during deposition. The cathode and magnetron gun both can be connected to different power supplies like DC, pulsed DC, to get the desired film deposition

condition. There are a number of power supplies which can be used for film deposition. A Trivac D16B roughing pump is used to pump down the chamber to a pressure of 8 mTorr and after that, a Pfeiffer HiPace 300 turbo pump is used to pump down to a lower pressure. Before starting of deposition, chamber is pumped down to 6.5 x 10^{-6} Torr pressure to get good quality film without any contamination from the atmosphere. A MKS Baratron gauge is used to measure the pressure up to 0 mTorr. To measure the pressure below that, an ion gauge IG2200 from Kurt J. Lesker is used. During the deposition water is circulated in the magnetron gun to avoid sticking of target to magnet. A Thermocouple gauge is also attached in line to get the line pressure and make sure that turbo pump is always under vacuum conditions. Gas flow is controlled by a MKS mass flow controller which can flow up to 100 sccm of any gas in precise manner.

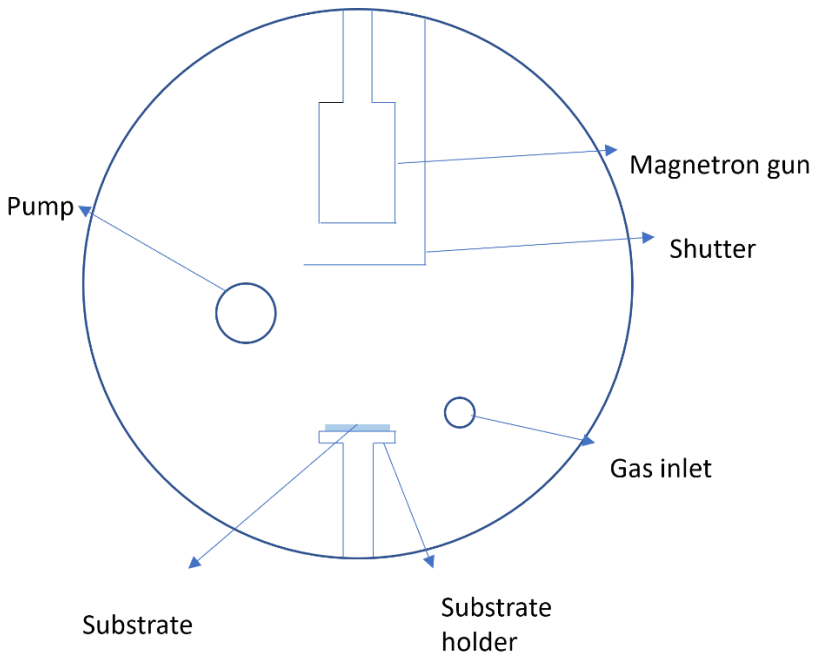

Figure 10: System schematic of PECVD coupled with magnetron gun

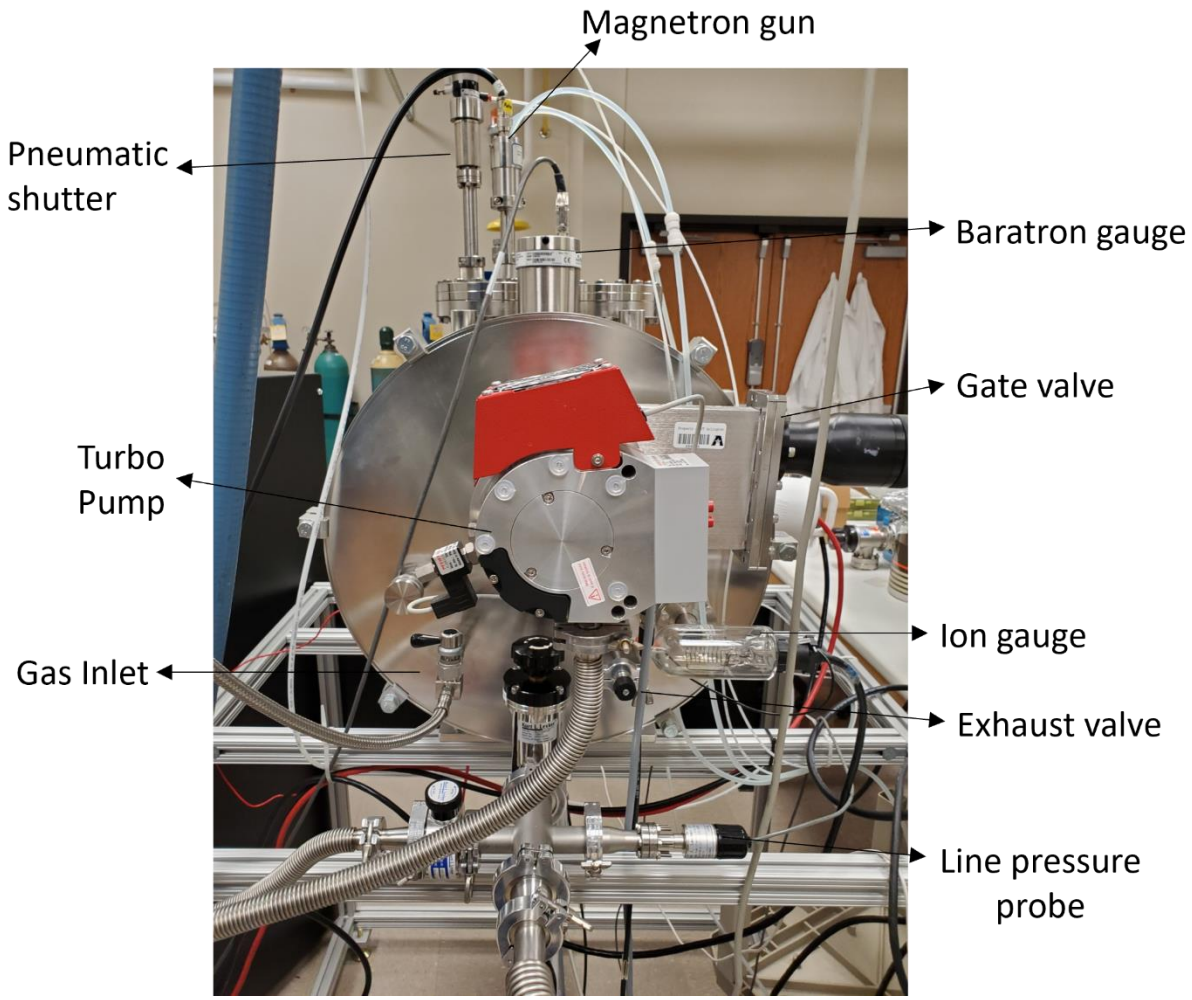

Figure 11: Back of PECVD chamber

In Figure 12, the space between two steel disks is visible. As discussed earlier, the outer part of that rod is shielding connected with ground and the inner part is the cathode. The bottom steel disk is in contact with the shield and the top with the cathode (substrate). To get plasma, 2-5 mm gap should exist between the disks. When a bias is applied in vacuum with Ar gas, due to voltage difference between the shield and cathode, plasma is generated.

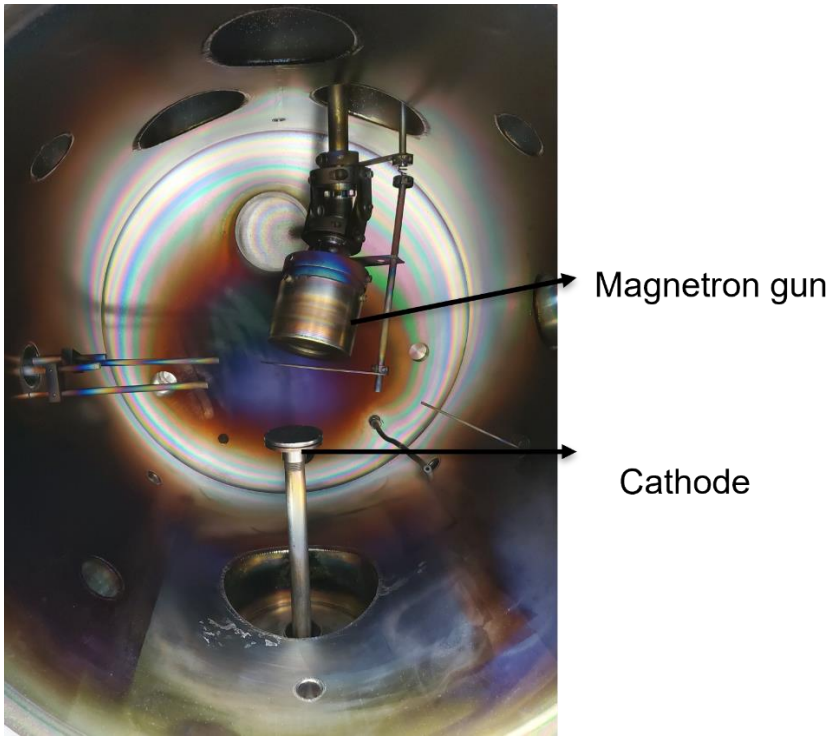

Figure 12: Inside of chamber

4.2 Procedure for DLC and Mo-DLC Deposition

4.2.1 Deposition of DLC

DLC and metal doped DLC have been studied in our lab over the last decade. During the deposition of film, some parameters play an important role which can be varied depending on the film characteristic requirements. The Si wafer with <100> orientation has been used as substrate in all depositions. A small area is marked with a marker on Si wafer to prevent DLC deposition allowing film thickness measurement after deposition. As discussed ahead, for all depositions the base pressure has been set to 6.5×10^{-6} Torr. The parameters which can be varied are, working pressure, total gas flow rate, methane proportion in total gas flow, power supply type and voltage bias on cathode. For DLC deposition, we have used two different types of power supply. These were Glassman DC power supply and Advance energy pinnacle pulsed DC power supply. The deposition parameters for DLC films are shown in Table 2.

Table 2: Deposition parameters for DLC

Name	Working pressure	Total gas flow (sccm)	Methane proportion	Power supply	Bias
DLC-1	20 mTorr	60	80%	DC	-650 V
DLC-2	20 mTorr	120	80%	DC	-650 V
DLC-3	20 mTorr	120	80%	DC	-1000 V
DLC-4	20 mTorr	60	80%	Pulsed DC	-650 V with 100 kHz frequency
DLC-5	20 mTorr	120	80%	Pulsed DC	-650 V with 100 kHz frequency
DLC-6	30 mTorr	60	80%	Pulsed DC	-650 V with 100 kHz frequency
DLC-7	30 mTorr	120	80%	Pulsed DC	-650 V with 100 kHz frequency
DLC-8	30 mTorr	60	80%	Pulsed DC	-650 V with 60 kHz frequency

DLC-9	30 mTorr	120	80%	Pulsed DC	-650 V with 60 kHz frequency
DLC-10	30 mTorr	50	25%	Pulsed DC	-650 V with 60 kHz frequency

4.2.2 Deposition of Mo-DLC

Mo is doped in DLC with magnetron sputtering during deposition. A pure Mo target of 99.5% purity with 0.250" thickness and 2" diameter is used for that purpose. The deposition parameters are shown in Table 3. For the deposition of Mo-DLC the total gas flow was fixed to 50 sccm. If pulsed DC is applied on the target, the repetition frequency is set at 100 kHz and pulse width is 2.5 µs. For pulsed DC on substrate, repetition frequency is set to 60 kHz and pulse width is 2.5 µs.

Table 3: Deposition parameters for Mo-DLC

Name	Working Pressure	Methane Proportion	Substrate Bias	Target Power
Mo-DLC 11	20 mTorr	10%	-1000 V DC	45 W pulsed DC
Mo-DLC 12	20 mTorr	10%	-1000 V DC	13 W pulsed DC
Mo-DLC 13	20 mTorr	15%	-1000 V DC	45 W pulsed DC
Mo-DLC 14	20 mTorr	15%	-1000 V DC	20 W pulsed DC
Mo-DLC 15	20 mTorr	15%	-1000 V DC	14 W pulsed DC
Mo-DLC 16	20 mTorr	25%	-1000 V DC	45 W pulsed DC
Mo-DLC 17	30 mTorr	25%	-1000 V DC	45 W pulsed DC
Mo-DLC 18	30 mTorr	25%	-1000 V DC	49 W pulsed DC
Mo-DLC 19	30 mTorr	25%	-1000 V DC	55 W pulsed DC
Mo-DLC 20	30 mTorr	25%	-1000 V DC	70 W pulsed DC

Mo-DLC 21	30 mTorr	25%	-1000 V DC	80 W pulsed DC
Mo-DLC 22	30 mTorr	25%	-1000 V DC	90 W pulsed DC
Mo-DLC 23	30 mTorr	25%	-650 V pulsed DC	49 W DC
Mo-DLC 24	30 mTorr	25%	-650 V pulsed DC	55 W DC
Mo-DLC 25	30 mTorr	25%	-650 V pulsed DC	60 W DC
Mo-DLC 26	30 mTorr	25%	-650 V pulsed DC	70 W DC
Mo-DLC 27	30 mTorr	25%	-650 V pulsed DC	80 W DC
Mo-DLC 28	30 mTorr	25%	-650 V pulsed DC	90 W DC
Mo-DLC 29	30 mTorr	25%	-650 V pulsed DC	120 W DC

4.3 Characterization of DLC and Mo-DLC

4.3.1 Deposition rate, roughness, and residual stress

Film thickness is measured with WYKO NT1000 surface optical profilometer. 5x lens and VSI mode was used to measure the roughness and thickness of film. The marked part of substrate was cleaned with ethanol. In that part, the height difference between the substrate and film was measured with optical profilometer. For both surface roughness and thickness of the film, 5 measurements were conducted. Effect of working pressure, total gas flow, methane proportion in total gas flow has been studied. The Atomic Force Microscopy (AFM) images were taken for Mo-DLC 18 and Mo-DLC 21 for 3 μm x 3 μm size with Parks System AFM. The deposition rate was calculated by dividing the thickness of the film by the deposition time. The curvature of substrate before and after deposition was calculated for DLC-10, Mo-DLC 17, Mo-DLC 18, Mo-DLC 19, Mo-DLC 20, Mo-DLC 21, Mo-DLC 22 with the same piece of equipment. Based on the curvature, film thickness and other parameters in Stoney's equation the residual stress was calculated. Stoney's equation is as follows.

$$\sigma = \frac{E_s\, d_s^2}{6(1-v_s)} \frac{1}{d_f}\left(\frac{1}{R_a} - \frac{1}{R_b}\right) \qquad (2)$$

where, E_s = Elastic modulus of substrate. In this case silicon wafer

d_s = Thickness of substrate

d_f = Thickness of film

v_s= Poisson's ratio of substrate

R_a = Radius of curvature of substrate after deposition

R_b = Radius of curvature of substrate before deposition

4.3.2 Structural characterization methods

4.3.2.1 SEM

All the samples have been examined using Hitachi H-3000N SEM for surface finish and any surface defects. To prevent damage to film, the imaging was done at 5 kV of acceleration voltage. EDS was conducted for all Mo-DLC samples to determine the Mo content. Other reason to use a low acceleration voltage is to prevent any signal from substrate.

4.3.2.2 XRD

All Mo-DLC films were analyzed using X-ray diffraction pattern in Bruker D-8 XRD diffractometer. Cu is used in tube as X-ray source producing wavelength of 1.54 Å. 50 kV and 40 Amps are used as acceleration voltage and acceleration current. To prevent the signal detection from substrate, low angle method is used. In low angle diffraction, the tube is fixed at low angle such that X-rays do not penetrate too deep into the sample. The detector is moved from across the angle range to collect the refracted x-rays. For these samples, the tube angle was set to 3° and detector was set to 27°. The X-ray diffraction pattern was collected for 30° to 50° using a step size of 0.01 and scan rate of 1 step/sec. Based on XRD pattern, using FWHM principal, approximate grain size was calculated.

4.3.2.3 TEM

Films of Mo-DLC 18 and Mo-DLC 21 were deposited on Cu support grid for TEM analysis. These films were analyzed by a Hitachi H-9500 HRTEM at 300 kV. Examination was conducted to determine the distribution of Mo in DLC matrix. Selected Area Electron Diffraction (SAED) pattern analysis was conducted on these 2 samples to better understand film structure.

4.3.2.4 Raman spectroscopy

Raman spectroscopy gives important information regarding the amorphous film structure due to its ability to differentiate between sp^2 and sp^3 bonding types. Raman measurements were obtained using the laser of 532 nm with 3 mW power to avoid possible beam heating effect. Raman spectra bands are fitted using gaussian fit.

4.3.3 Characterization of mechanical and tribological properties

4.3.3.1 Nanoindentation

The Hysitron Ubi 1 nano indenter has been used to measure film hardness and indentation module. DLC and Mo-DLC has been deposited on Si wafer for a minimum of 1100 nm of thickness. The indentation tests were conducted in depth control manner such that maximum depth of indent is not more than 10% of total thickness. Depth is kept below 10% of film thickness to avoid any effect of substrate on film hardness. All the samples have been tested for 9 indents of the same depth.

4.3.3.2 Pin on disk experiments

Pin on disk tribotest were conducted to study the friction coefficient and wear rate of the films. A Ball made of 440 C is being used as pin material and constant load of 5 N is applied. These tests are performed in a laboratory environment. Sliding velocity has been kept to 5 cm/s and the total distance travelled at 1000 m for each test. The friction coefficient has been observed as a function of sliding distance. The same test has been performed with high performance 80W-90 gear oil lubrication. In the pin on disk experiments, all the films had minimum thickness of 1800 nm.

After the experiment, the wear track has been observed in optical profilometer and SEM/EDS. From the 2-D profile of the wear track, volume loss has been calculated. Specific wear rate is calculated using the following equation.

$$wear\ rate = \frac{wear\ volume\ (mm^3)}{Load\ (N) * Sliding\ Distance\ (m)} \quad (3)$$

After testing, the pin was also observed under SEM/EDS.

CHAPTER 5

RESULTS AND DISCUSSION

5.1 Deposition Rate, Roughness, and Residual Stress

First, a study was conducted to determine appropriate processing conditions for DLC and Mo-DLC films. DLC-1, DLC-2, have been deposited at -650 V DC bias. When DC bias is used on the cathode, there is a tendency for charge to build up. During the deposition of these films, for the first 2 minutes a very weak plasma was generated which eventually was extinguished. This means that at -650 V DC bias, there is not enough energy on the cathode which can be transferred to the gas to get it ionized and create strong plasma. DLC-3 was deposited at -1000 V DC bias which resulted in to weak but stable plasma. The deposition rate was 7 nm/min. The rest of the DLC films were deposited with -650 V pulsed DC bias. The SEM images of DLC-6 and DLC-8 are shown in Figure 13. DLC-6 was deposited with 100 kHz repetition frequency while DLC-8 was deposited with 60 kHz frequency.

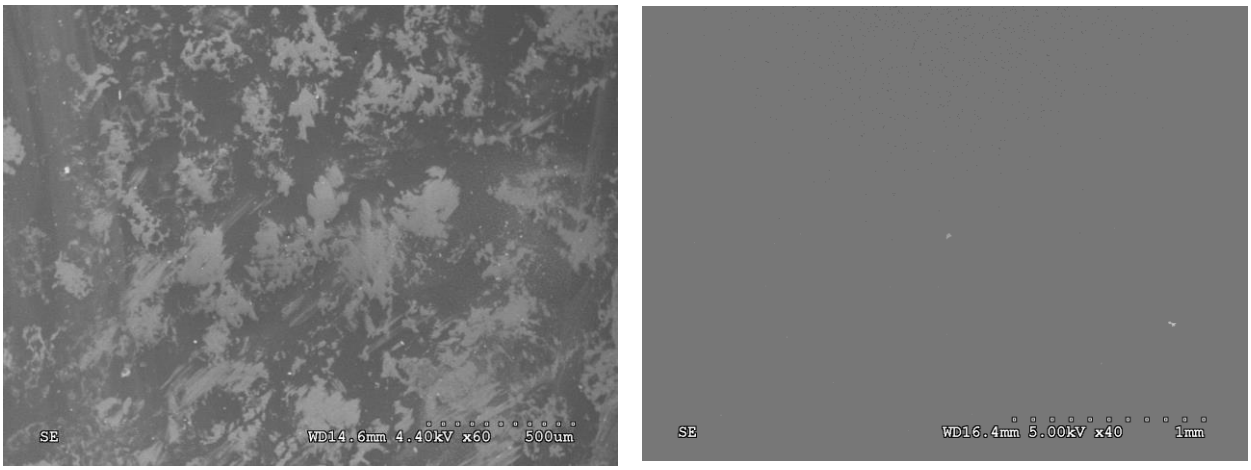

Figure 13 (a) and (b) : SEM images of DLC-06 and DLC-08

During the deposition of DLC-6, more power is generated at the substrate due to higher frequency. Higher power leads to re-sputtering of deposited film which results into mountain like structures as seen in Figure 13 (a). To solve the problem repetition frequency was lowered to 60 kHz which resulted into smoother film at 20% more deposition rate. Figure 13 (b) shows a SEM image of DLC-8 which is deposited at 60 kHz repetition frequency keeping all other parameters the same. Despite the difference in working pressure, total gas flow rate films deposited at 100 kHz, DLC-4, DLC-5, DLC-7 showed the mountain like structures as well.

At 30 mTorr pressure, change in total gas flow rate from 60 sccm to 120 sccm has no significant effect on deposition rate. Which means that at 30 mTorr and 60 sccm total gas flow, ions are taking all the energy available from the cathode.

When Mo-DLC was tried to be deposited at 30 mTorr, 60 sccm total gas flow with 80% methane in the gas, Mo content in the film became an area of concern. Mo was not incorporated into the DLC even at higher applied power on target. Also, micro arcing was taking place between the shield and target in small gap which was not getting detected by power supply. A thin carbon layer was getting deposited on the target which subsequently was transferred to the substrate, Figure 14. So, when the power was applied to the target, carbon atoms were deposited on the target and they were sputtered to the substrate instead of Mo from the target. EDS analysis was also conducted on the target after deposition, which also revealed formation of a thin layer of carbon. To avoid carbon deposition and increase the amount of Mo in the film, the methane proportion in the total gas was reduced to 10%, 15%, 25%.

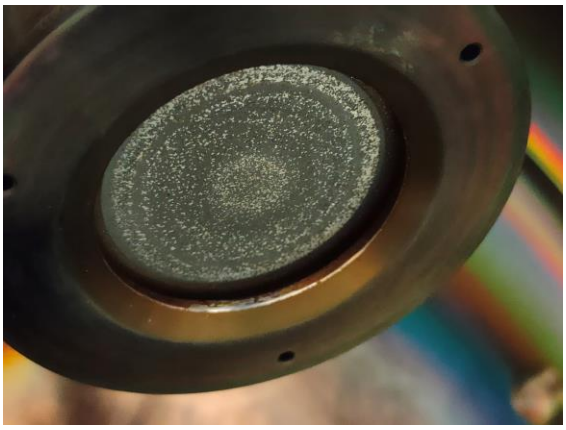

Figure 14: Carbon layer deposition on target

Under these conditions, formation of a carbon layer was still present even at 10%, 15% and 25% methane, but a substantial amount of Mo was obtained in the DLC film. To further improve the deposition quality, the target was cleaned with acetone and no carbon was left on the target before each deposition.

Film deposition rate, and Mo content for different methane proportions of the gas flow is shown in Figure 15. The graph shows data from Mo-DLC 11, 12, 13, 14, 15, 16.

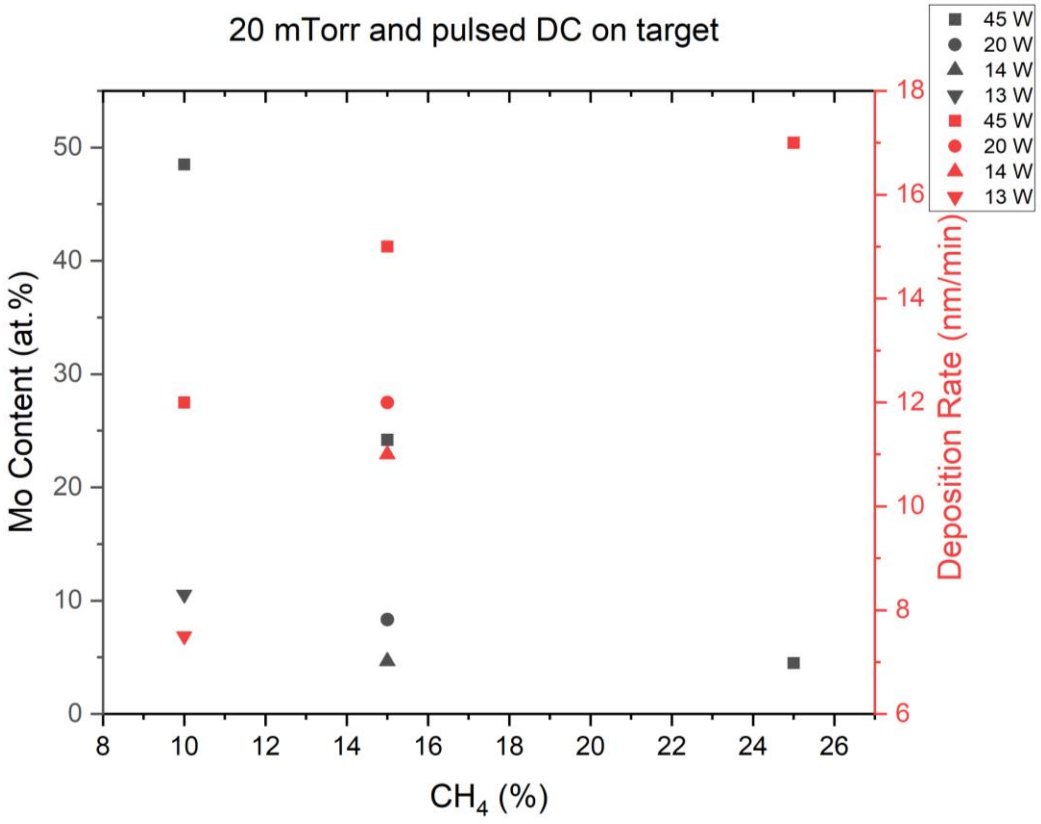

Figure 15: Effect of methane proportion on Mo content and deposition rate

The lowest Mo content at 10% methane is 10 at.% at 13 W pulsed DC power. If a lower power is used on the target, there is no plasma generation. So, at 10% methane, 10 at.% Mo is the lowest Mo content which can be obtained. The deposition rate is also low, around 7 nm/min. The same situation exists for the 15% methane. Compared to 25% methane in total gas flow, both 15% and 10% have shown poor control over Mo content over the range of applied power with lower deposition rate. DLC-10 was deposited with 25% methane to compare the properties of non-doped DLC and doped DLC.

The effect of working pressure on deposition rate, hardness and roughness has also been explored, Figure 16.

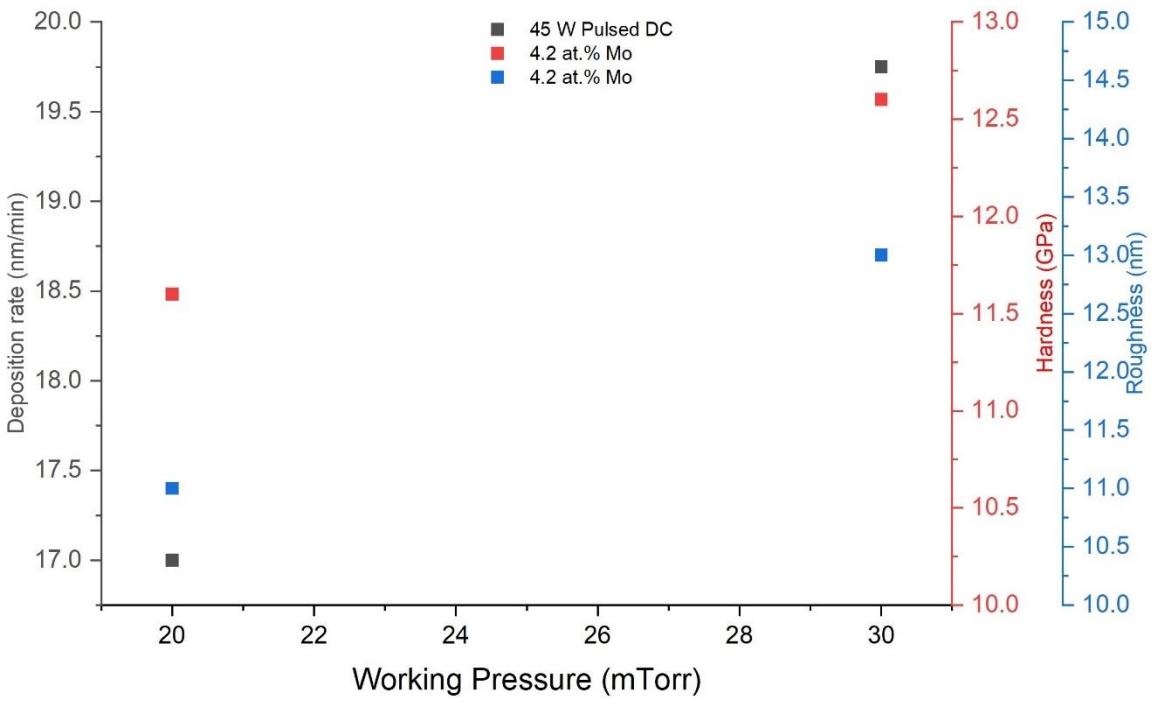

Figure 16: Effect of working pressure on hardness deposition rate and roughness

The graph shows the data for samples Mo-DLC-16 and Mo-DLC 17. Both films were deposited with same power on target. Only difference was the working pressure. Working pressure did not affect the Mo content in film. Deposition rate was increased from 17 nm/min to 19.75 nm/min resulting 18% increase for the higher working pressure of 30 mTorr. Hardness and roughness were also increased for deposition at 30 mTorr but the benefit of hardness increase outruns the drawback of small roughness increase. It changed from 11 nm to 13 nm which is not a significant change.

Two films with different Mo content were examined with AFM to determine if the Mo content affects the roughness. Figures 17 and 18 show the AFM images of Mo-DLC 18 and Mo-DLC 21 with 4.2 at.% Mo and 11.8 at.% Mo, respectively.

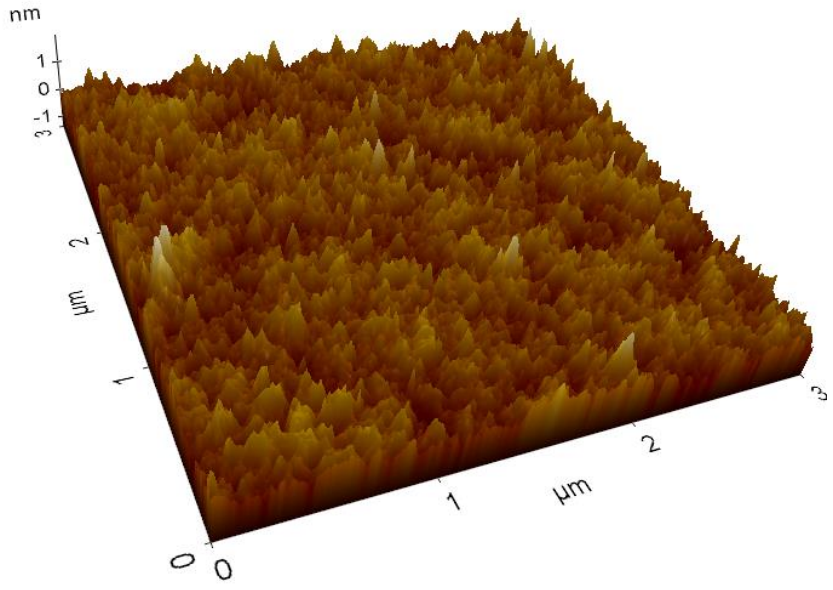

Figure 17: AFM image of Mo-DLC 18 (4.2 at.% Mo)

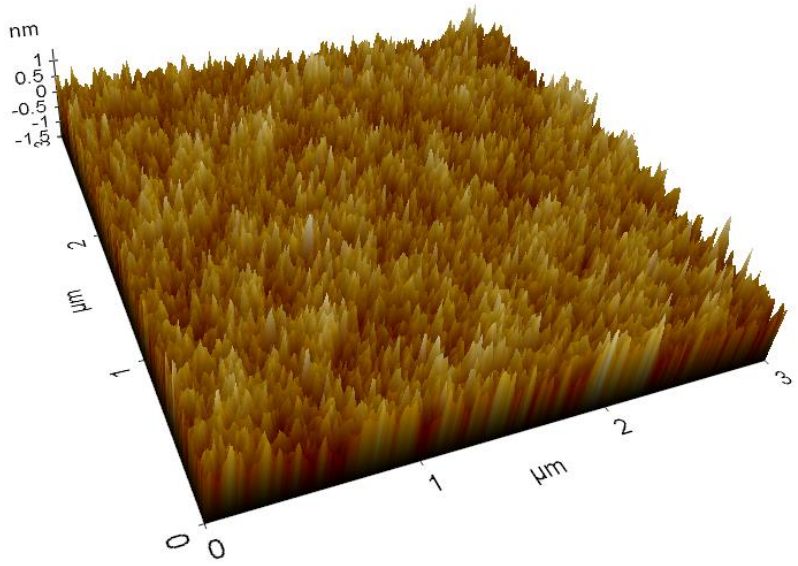

Figure 18: AFM image of Mo-DLC 21 (11.8 at.% Mo)

The average roughness value for Mo-DLC 18 and Mo-DLC 21 is 14 nm and 17 nm, respectively. The AFM images show a very similar surface profile for both films despite the difference in metal content.

Residual stresses in the film were found to decrease with increasing metal content, Figure 19. For non-doped DLC, the residual stress was 1.5 GPa which was reduced to 0.4 GPa for 16.9 at.% Mo in film. With the metal doping, sp^3 bonds are broken which leads to reduced residual stress in film as has been observed in previous other Me-DLC systems [17, 34, 36, 37, 38, 41, 44, 49].

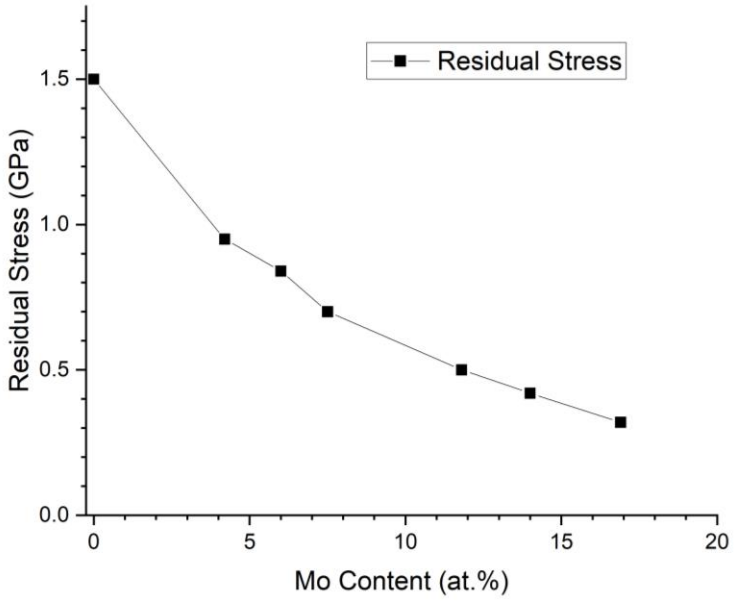

Figure 19: Residual stress vs. Mo content

.

5.2 Effect of Power Supply on Mo Content and Deposition Rate

Figure 20 shows the effect of target power on deposition rate and Mo content. Also, it shows the effect of different power supply on deposition rate and Mo content in film.

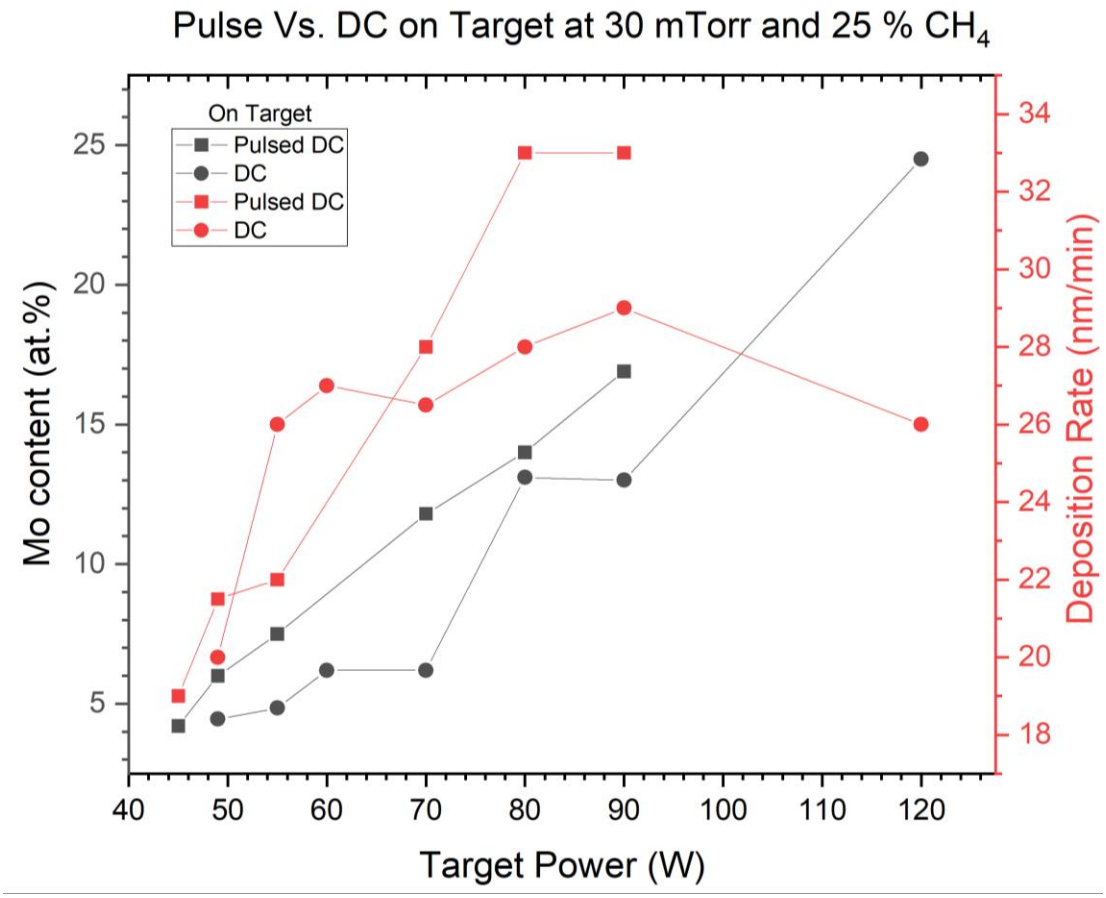

Figure 20 : Effect of target power on deposition rate and Mo content

Mo content is increased with power for both pulsed DC and DC both. The Mo content increase with pulsed DC power seems to be more consistent compared to DC power. For same power from pulsed DC and DC, Mo content was nearly same while deposition rate for pulsed DC was higher than DC. As it is seen, both power supplies showed a plateau in terms of deposition rate. DC showed that plateau much earlier (29 nm/min) than pulsed DC (33 nm/min). It is

interesting that the higher plateau of deposition rate for pulsed DC was obtained at almost the same power (at around 80 W). Charging effects prevailing in the DC power might be the reason behind it. In pulsed DC, charging is suppressed allowing a higher deposition rate to be realized.

5.3 X-ray Diffraction Pattern

XRD patterns of Mo-DLC films over different Mo contents are shown in Figure 21. The result show that at a low Mo content around 4.2 at.% no diffraction peak were observed. Formation of two weak peaks takes place at Mo content around 6 at.%. The intensity of these two peaks increases with increase in Mo content. The two peaks have a d-spacing of 2.49 Å and 2.16 Å corresponding to 2Θ 36.01° and 41.9°, respectively. These d-spacing values match well with the (111) and (200) planes of the cubic MoC in cubic phase (PDF-40-021-2527 and PDF-04-001-2968). M. Constantinou et al. [10] reported reaction between Mo and C from DLC at 2 at.% and higher Mo content resulting in formation of MoC. Thus, the evidence shows that beyond a content of 4.2%, Mo exists as MoC. The resolution of the XRD technique is not high enough to resolve the state of the Mo phase at Mo contents at and below 4.2 at.%.

The wider diffraction peaks observed in the XRD pattern are an indication of a small grain size. FWHM measurements were obtained from the XRD pattern after baseline correction and a mean grain size "r" was determined using equation 4.

$$FWHM = \frac{0.9*\lambda}{r*cos\theta} \qquad (4)$$

where λ is wavelength of X-ray waves (1.54 Å)

The grain size for Mo-DLC-19 (7.5 at.% Mo) and Mo-DLC 20 (11.8 at.% Mo) was determined to be 2.89 nm and 3.05 nm, respectively. This suggests that with increase in Mo, the MoC grain size does not increase significantly.

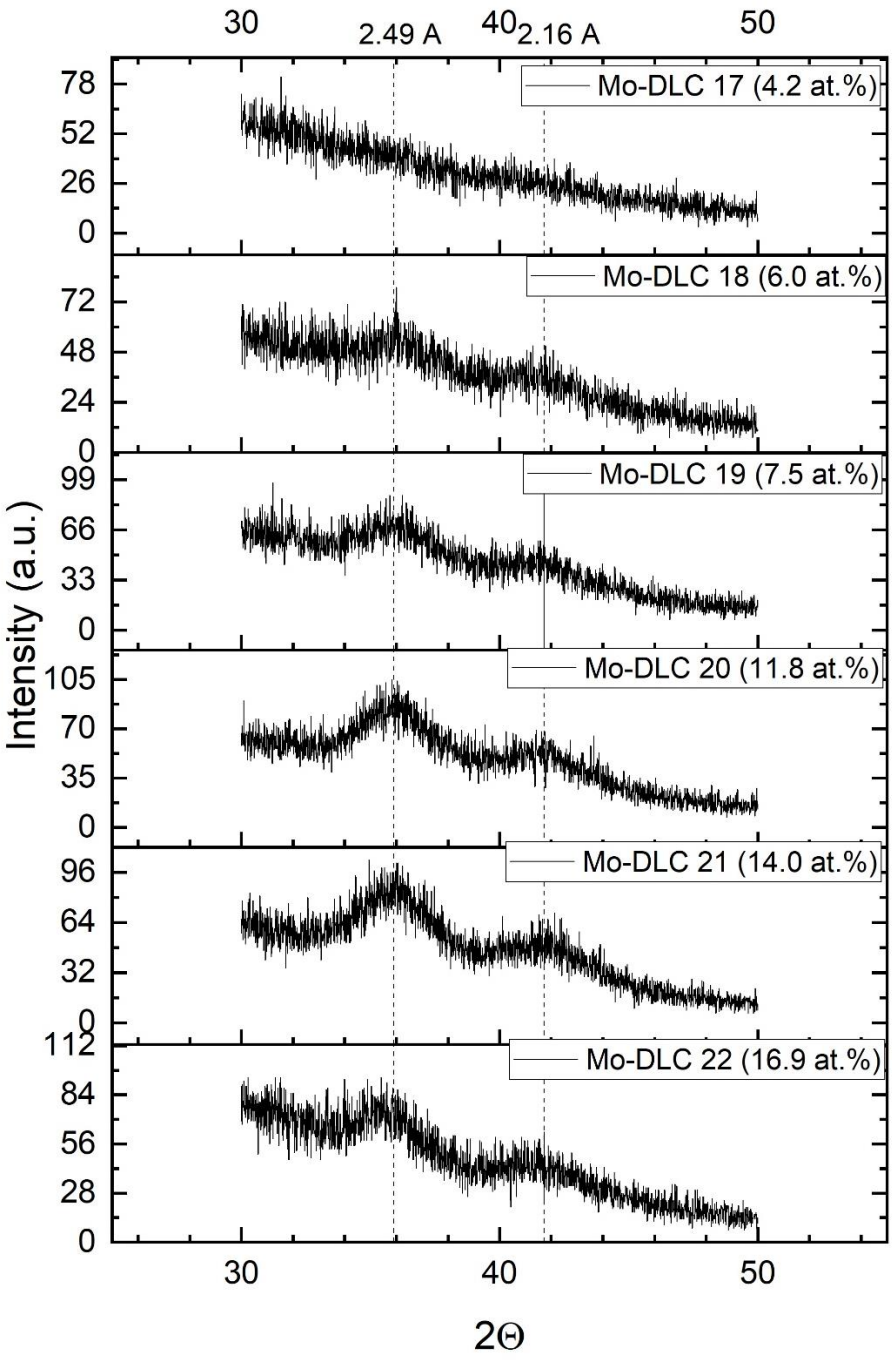

Figure 21: XRD pattern for Mo-DLC for different Mo content

5.4 TEM Analysis

Mo-DLC 17 and Mo-DLC 20 were examined with HRTEM. TEM images of both show darker spots surrounded by brighter boundaries, Figures 22 and 23. Darker spots are Mo-containing nano particles which are surrounded by amorphous carbon-rich boundaries. SAED patterns from Mo-DLC 17 and Mo-DLC 20 were also analyzed (insets in Figures 22 and 23). The d spacing of the diffraction rings was calculated and both films showed a cubic MoC phase in agreement with XRD results. These rings correspond to <111>, <200> and <220> orientation of planes for cubic MoC. Which means that, Mo forms MoC around 4.2 at.% as well but the amount of MoC phase might be too low to be detected in XRD. From the TEM images, it was concluded that the average grain size for 4.2 at.% Mo is around 2-2.25 nm and for 11.8 at, % Mo its around 3.10-3.15 nm. Actually, the latter grain size value is in agreement with the grain size calculation using the FWHM method. At higher Mo content, more MoC is formed but the MoC phase is still surrounded by graphitic boundaries.

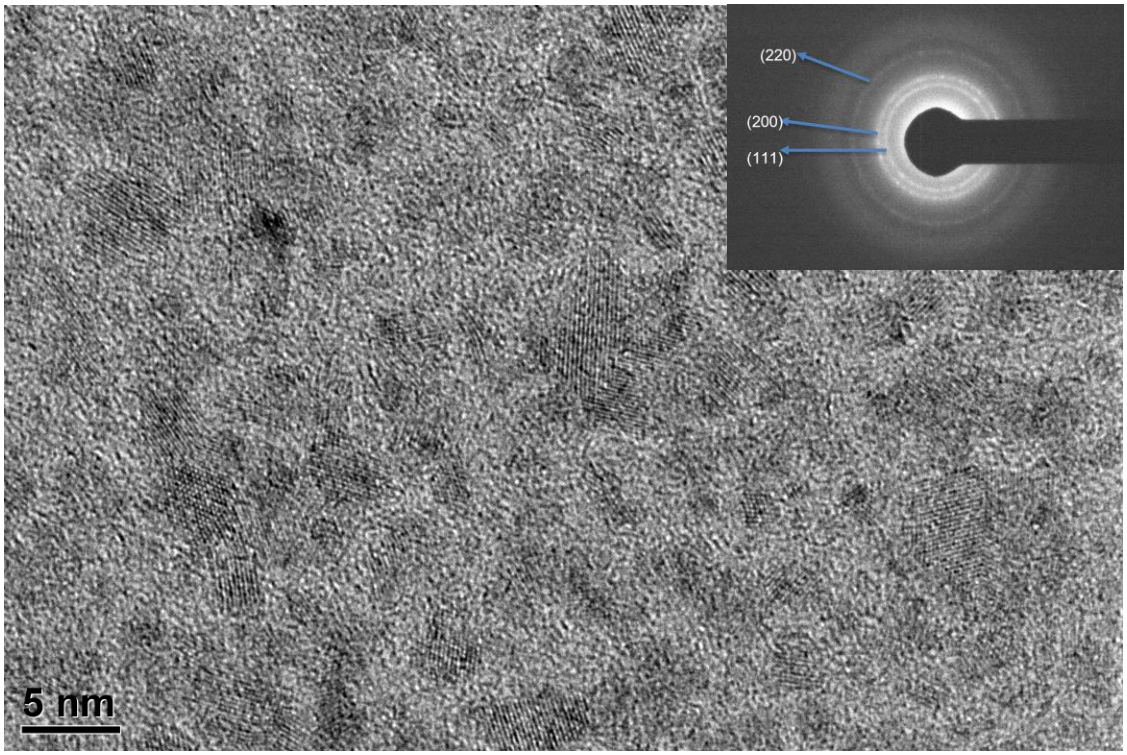

Figure 22: HRTEM image and SAED pattern for Mo-DLC 17

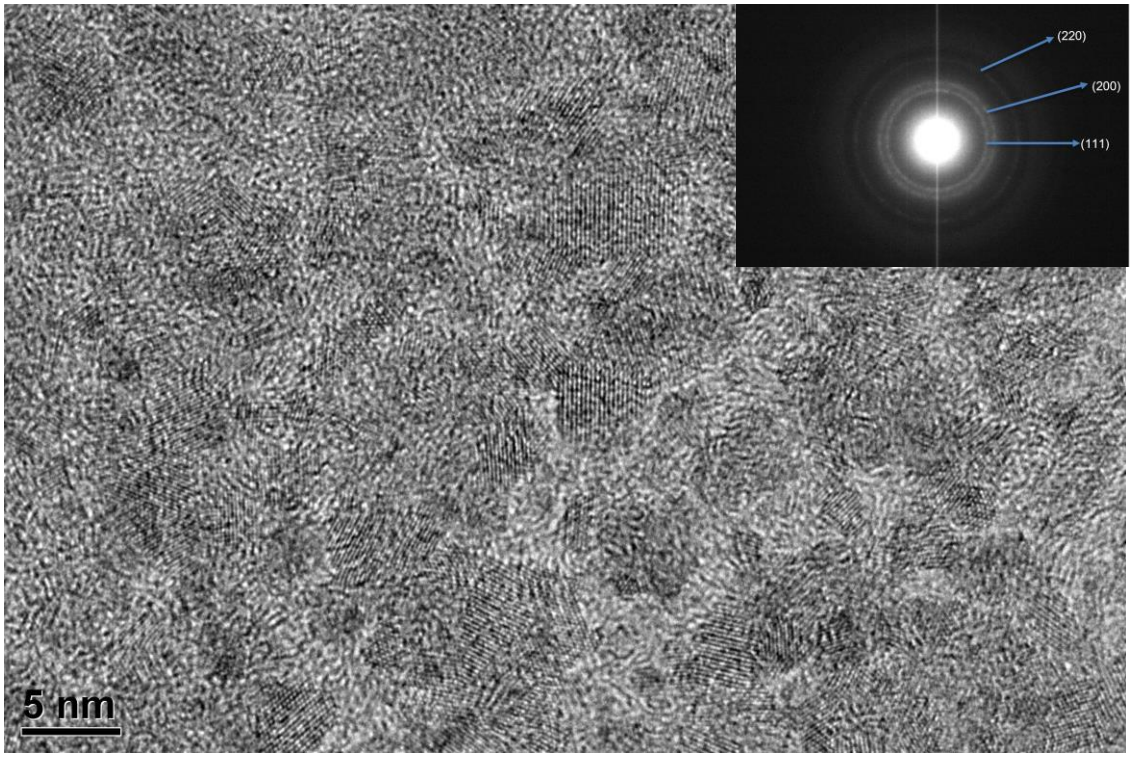

Figure 23: TEM image and SAED pattern of Mo-DLC 20

5.5 Raman Spectroscopy

Raman spectra provide the information about microstructure changes in the film with different metal content. Raman measurements were carried out using laser a of 532 nm with low input power of 3 mW to reduce the chances of possible beam heating effects. Raman spectra of films with various Mo contents are shown in Figure 24. All spectra were fitted with gaussian fit to get intensity data of both bands. Raman spectra of amorphous carbon consist of G peak and D peak around 1550 cm^{-1} and 1350 cm^{-1} respectively. The G peak is related to ordered sp^2 bonded carbons in film and D peak is related to disorder in the film. In this case disorder is related to sp^3 bonds. The intensity value of single D peak or single G peak does not give any indication. But when the ratio of intensity of D peak over G peak is taken into the account, it provides information related

to sp^2 and sp^3 bonds in film. Increase in I(D)/I(G) is related to increase in sp^2 bonds in the film. Also, position of G peak sifts towards higher wavenumber with increase in sp^2 bonds.

The Raman spectra in Figure 24 show that the D and G peaks are in range of 1370 cm^{-1} to 1380 cm^{-1} and 1550 cm^{-1} to 1565 cm^{-1}, respectively. With increase in Mo content, the D peak starts to appear a little sharper. Figure 25 shows the effect of Mo content on G peak position, FWHM of G peak and I(D)/I(G) ratio. The values of G peak position, FWHM and I(D)/I(G) ratio were obtained by deconvoluting the Raman spectra using gaussian fit. With increase in Mo content, I(D)/I(G) ratio increases which implies that with increase in Mo, formation of more sp^2 bonds is favored. There is no linear relation between increase in Mo content with increase in I(D)/I(G) ratio. The G peak shifts towards higher wavenumber with increase in Mo content. As it is seen, the relation between G peak position shifting and Mo content is not linear either. The G peak moved to lower wavenumber for 6 at.% Mo then it started to move to higher wavenumber up to 16.9 at.% Mo. However, no significant effect of Mo on D peak position was found. Regarding the FWHM of G peak, a general trend of decrease with increase in Mo content was seen. However, the relation is not linear either.

From the Raman spectra study of different metal doped DLC films, it was established that increase in I(D)/I(G) ratio, G peak shift towards higher wavenumber and FWHM decrease for G peak with increase in metal content are indications of metal contribution in more sp^2 bonded carbons in DLC films [42].

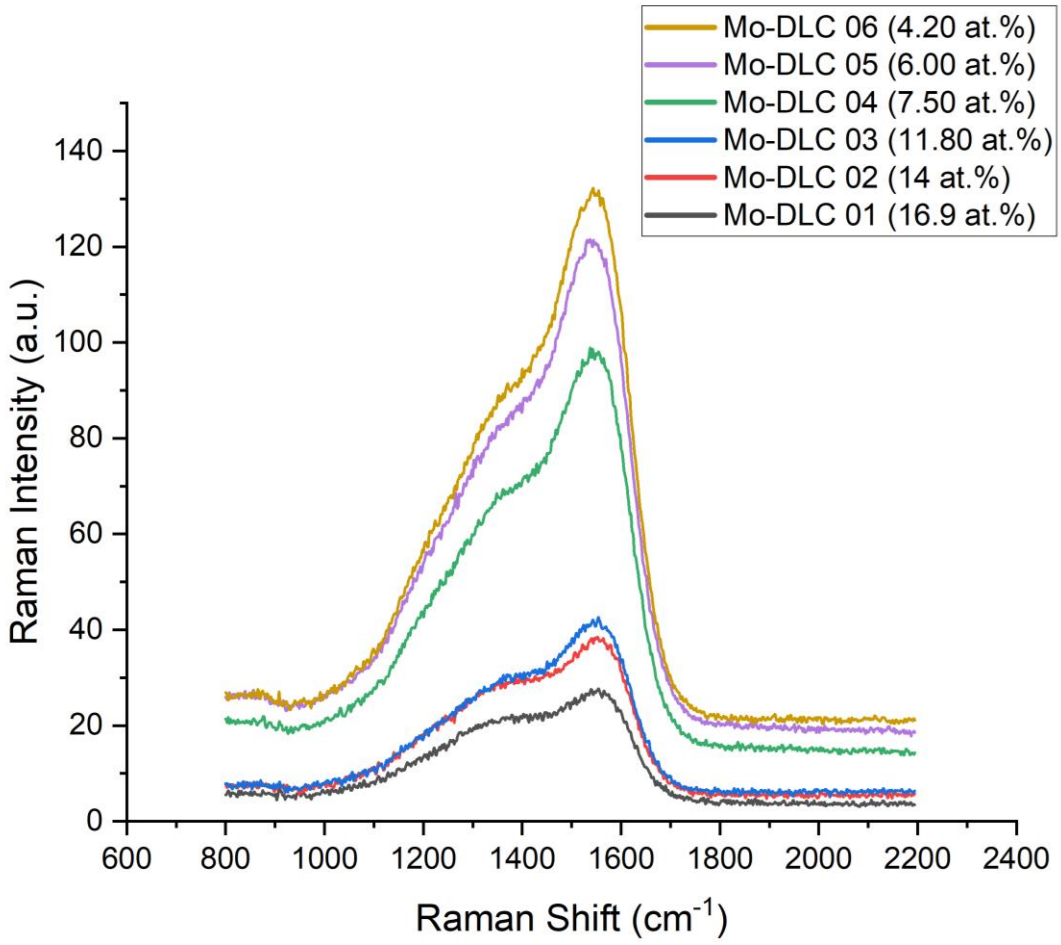

Figure 24: Raman Spectra for Mo-DLC

Table 4: Raman analysis data

Mo Content (at.%)	FWHM (G)	I(D)/I(G)	G peak wavelength
4.2	148.2	0.87	1553
6.0	148.3	0.89	1551
7.5	145.2	0.92	1553
11.8	139.0	0.96	1558
14	133.2	1.06	1561
16.9	133.5	1.12	1563

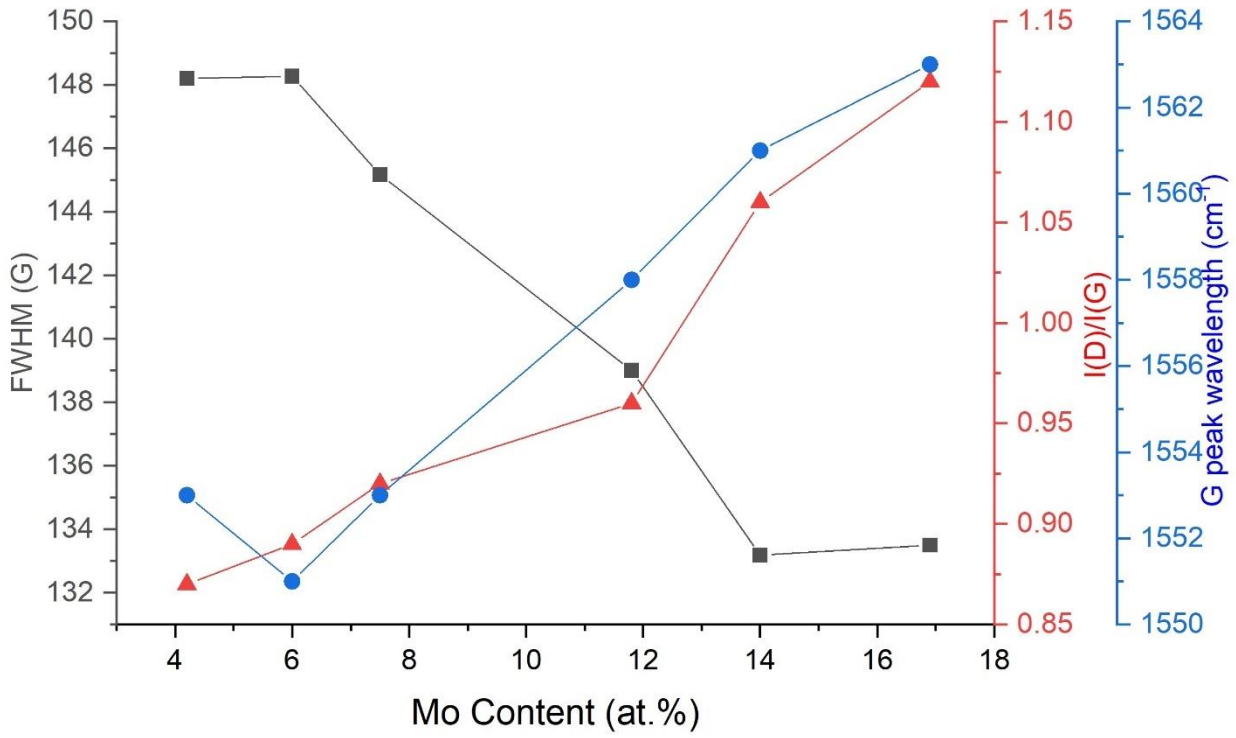

Figure 25: Effect of Mo content on FWHM, I(D)/I(G) ratio and G peak position

5.6 Nano Hardness and Elastic Modulus

Hardness of Mo-DLC films was determined with nano-indentation experiments under depth control mode. Total 9 indents were taken for all the films at different spots such that maximum depth of indent does not go above 10% of film thickness to avoid possible effect from substrate. Mo-DLC deposited with pulsed DC and DC power were tested for nano indentation and the change in hardness over Mo content is shown in Figure 26.

For both power supplies, change in hardness with Mo content is nearly the same. There is no significant difference in hardness for the same Mo content. It has been well established that hardness of DLC drops when doped with metal [17, 34, 36, 37, 38, 41, 44, 49]. It is noted that the

higher hardness of pure DLC film (14 GPa) is also associated with high residual stresses (~1.5 GPa), Figure 15. While in Mo-DLC films hardness are at insignificant level of residual stresses. Which means that one of the major concerns of residual stress in DLC film has been resolved with metal doping. With increase in Mo content, hardness of the film increases. From TEM and XRD analysis, it was clear that with increase in Mo content, more MoC is formed but by maintaining a nano level grain size. In this case, increase in hardness is because of more MoC phase nano grains in the film. MoC is hard phase.

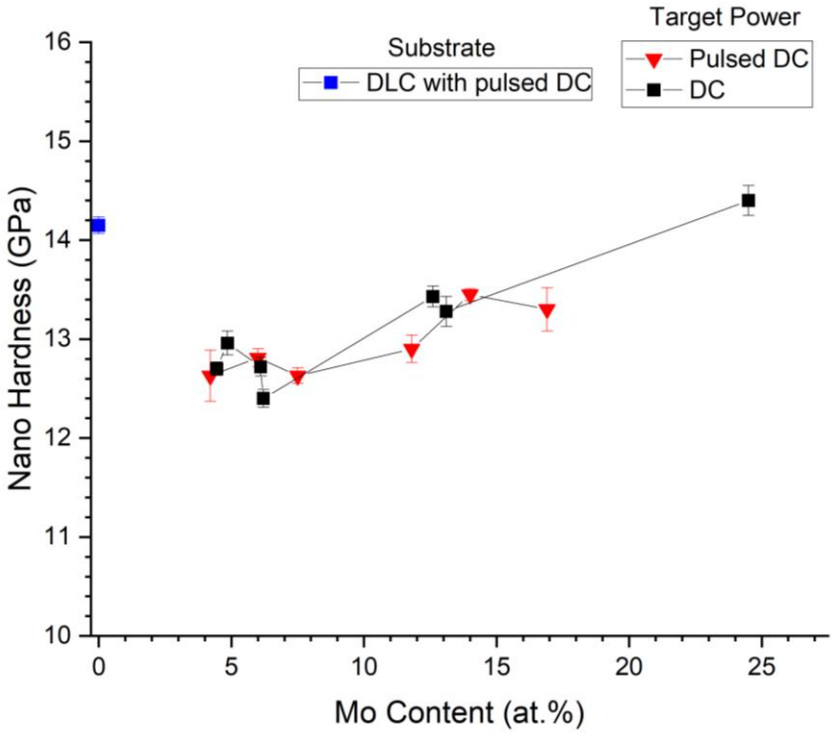

Figure 26: Effect of Mo content and power supply on hardness

Figure 27 shows the change in hardness and Young's modulus with change in Mo content. Elastic modulus increases with increase in metal content and a general trend for hardness is also upwards with increase in Mo content.

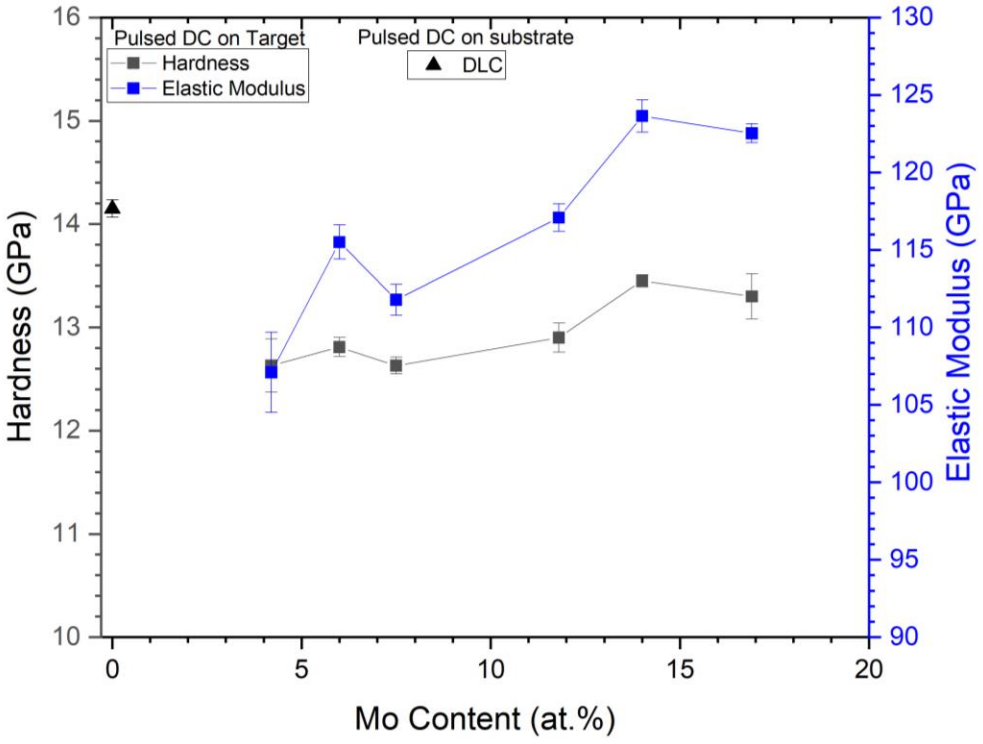

Figure 27: Hardness and elastic modulus variation with Mo content

5.7 Tribological Properties

Tribological properties of Mo-DLC and DLC have been studied in dry sliding and lubricated sliding conditions. Mo-DLC films with 2 at.%, 6 at.% and 16 at.% were tested. Figure 28 shows the COF variation for all tested samples. Friction coefficient of DLC was the lowest at 0.1 which increased to 0.42 at 2at.% Mo. Further increasing Mo content resulted to reduce the COF to 0.115 for 6 at.% Mo and 0.135 for 16 at.% Mo. It is interesting that all films except the one with 4.2 at.% Mo exhibited a steady state COF. On the contrary, the COF in this film increased to ~0.4 and never reached steady state. Figure 29 shows the specific wear rate and COF as a function of Mo content. After testing, all samples were analyzed with the optical profilometer to obtain wear track data. The wear track area was obtained from the 2-D profile of each wear track.

Volume loss was calculated by multiplying the wear track 2D area by the circular perimeter. Specific wear rate was calculated from ratio of volume loss over force and total sliding distance.

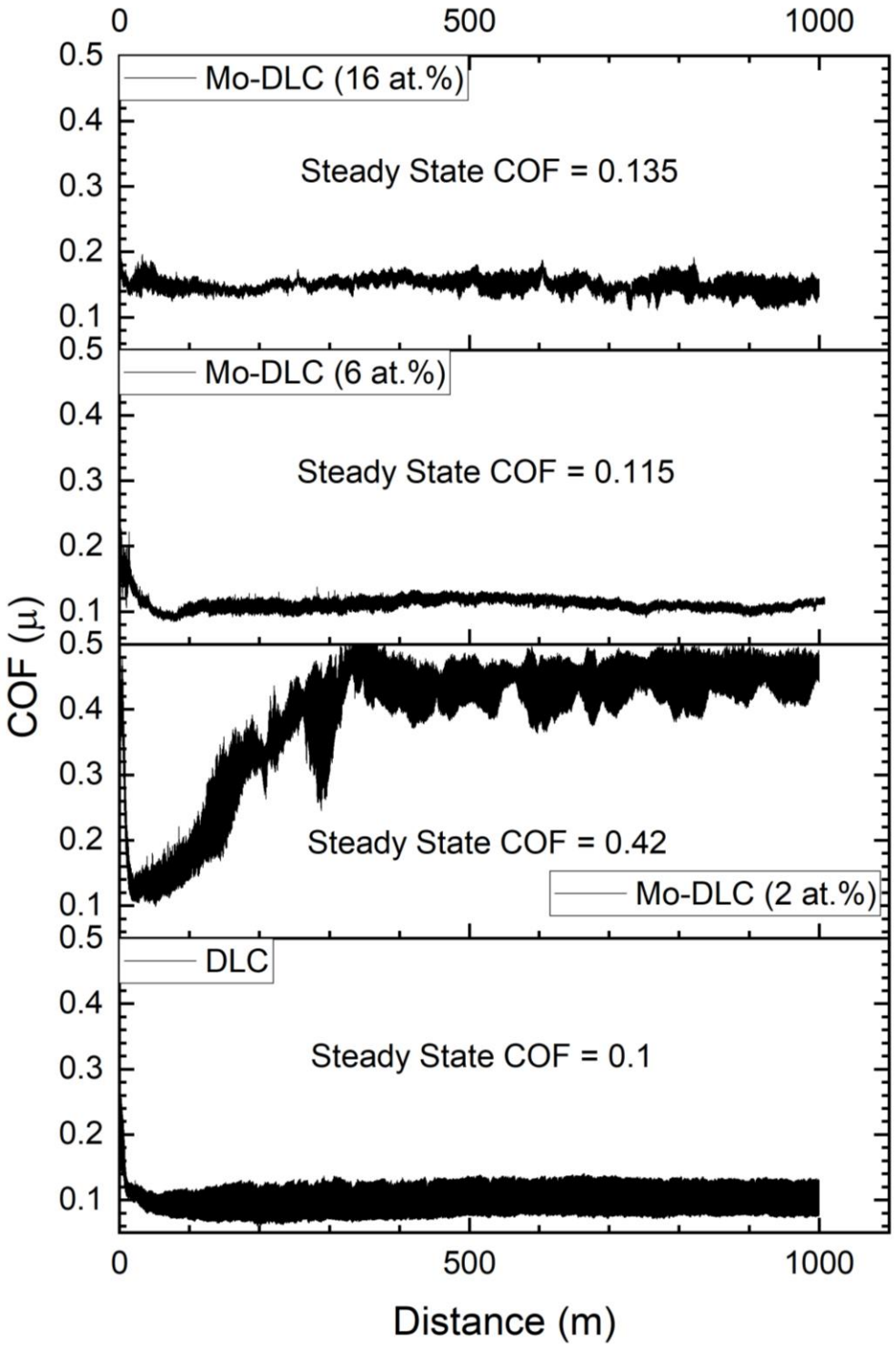

Figure 28: COF plot of DLC and Mo-DLC for dry sliding condition

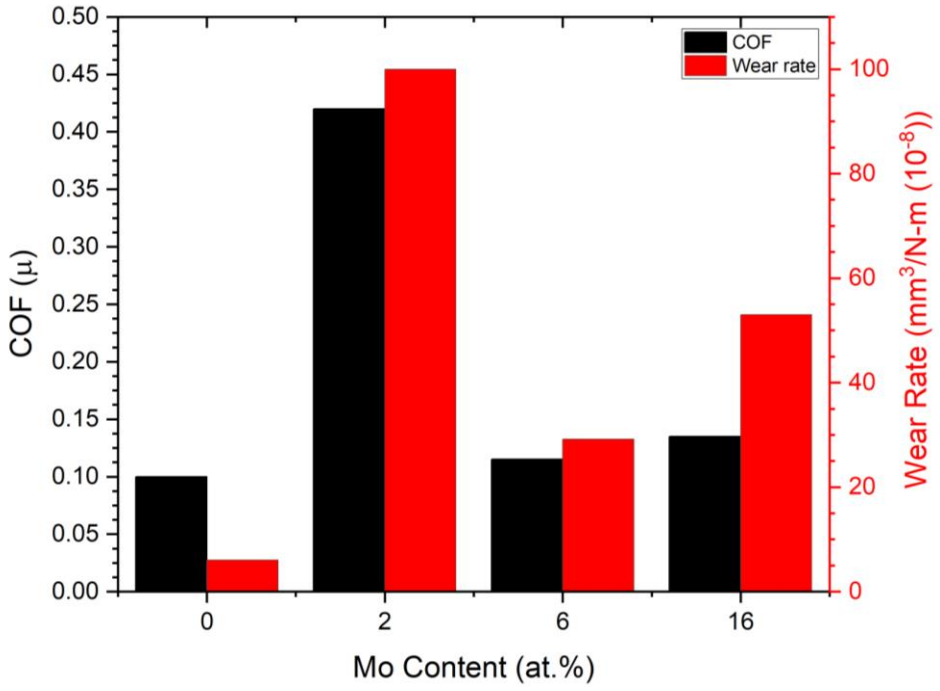

Figure 29: COF and wear rate of DLC and Mo-DLC for dry sliding condition

The COF and wear rate of 2 at.% Mo film is higher than any other film. The COF did not stabilize and exhibited an entirely different behavior. This response can be attributed to the presence of very small size MoC particles (~2 nm) which are in the initial stages of formation and possibly incoherent with the DLC matrix. Thus, this might have as a result the detachment of these particles from the DLC matrix and their introduction in the wear track which can cause the three-body wear. As a result of this process, continuous disruption in the graphitized layer can take place. The MoC phase at higher Mo contents may be more stable and coherent with the surrounding graphitic grain boundaries. This leads to formation of a more coherent transfer layer and producing a reduction in the COF.

Profilometry of all films showed that the pure DLC has the shallowest wear track. The depth of wear track increases with increase in Mo content. Figures 30, 31 and 32 exhibit the 3-D and 2-D profiles of all wear tracks.

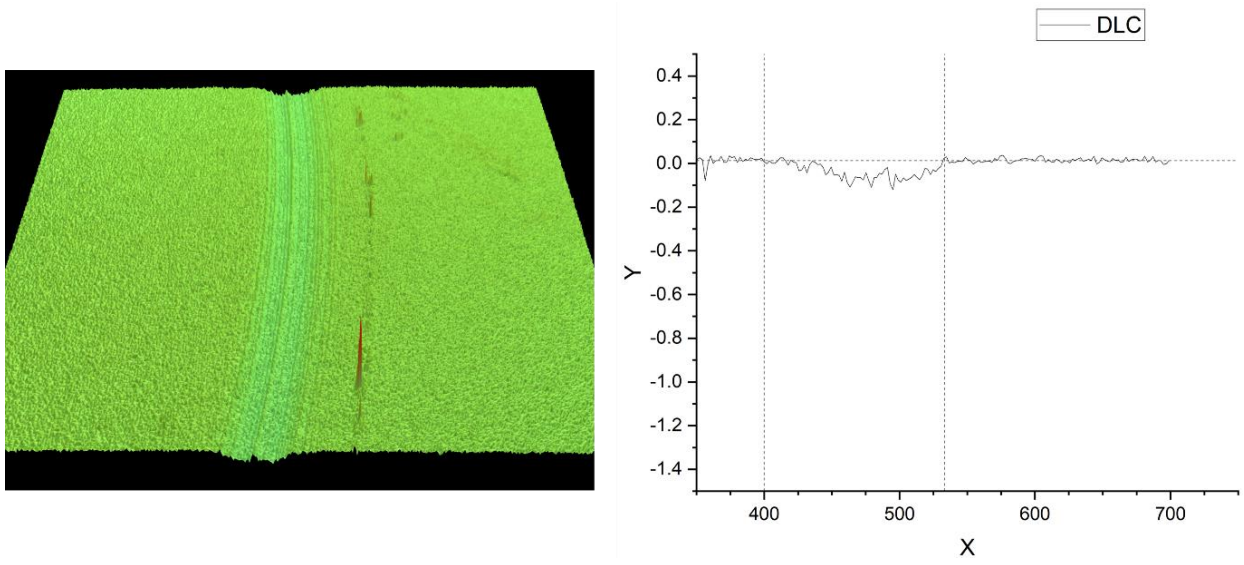

Figure 30: 3-D and 2-D wear track of DLC

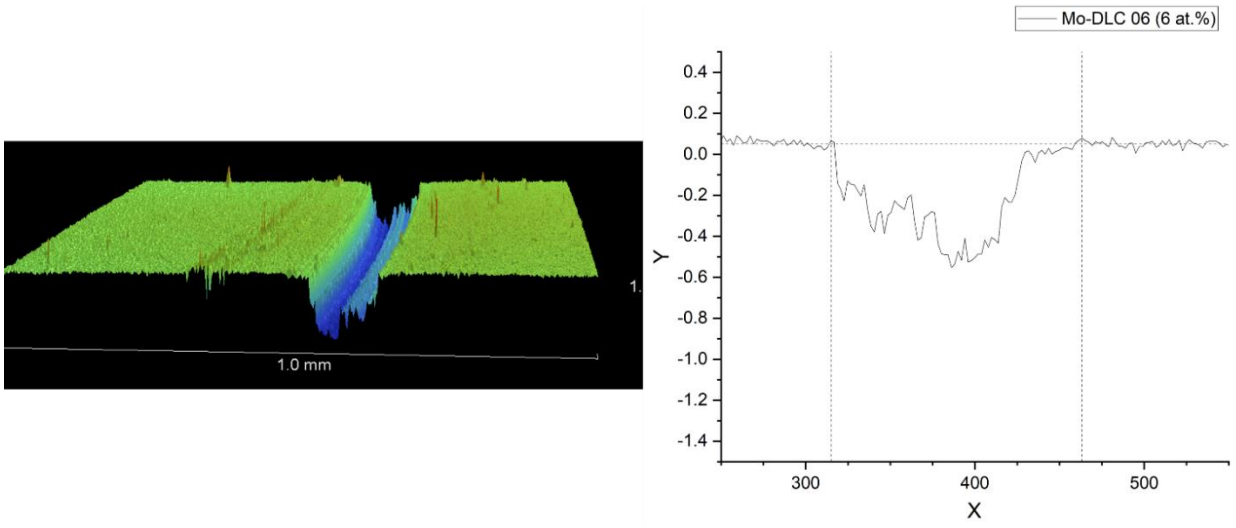

Figure 31: 3-D and 2-D wear track of Mo-DLC (6 at.%)

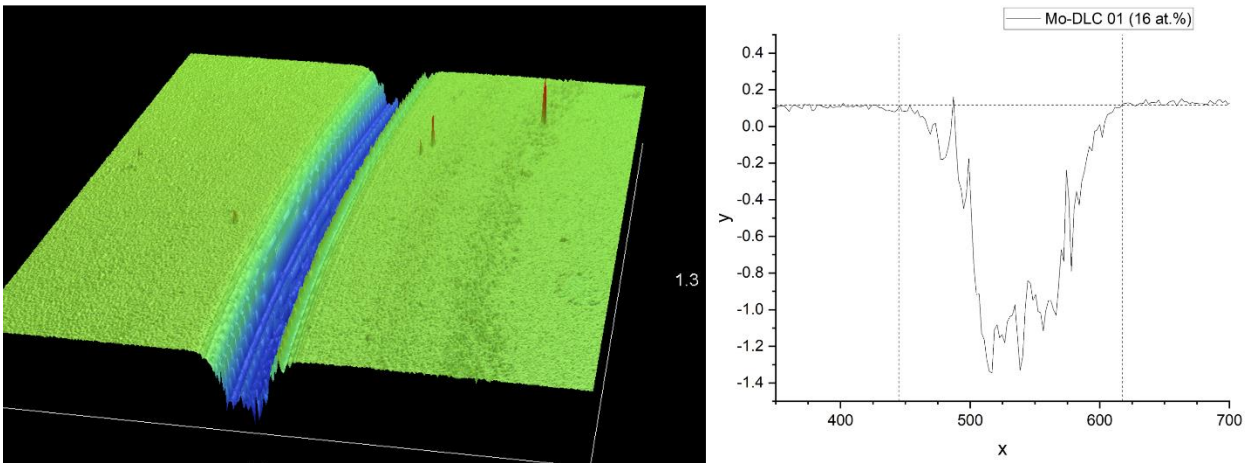

Figure 32: 3-D and 2-D wear track of Mo-DLC (16 at.%)

SEM and EDS analysis were conducted on the wear track of the Mo-DLC and ball. From the EDS results, it was clear that a film is transferred to the ball during testing. In this case, static partner is ball made from 440 C SS. EDS results of ball surface are shown in table 5. It is seen that Mo is there in significant amount accompanied by C. Mo-DLC is made out from Mo and C. Which suggests that the wear mechanism involves the transfer of film from the sample to the static partner. Figure 33 shows typical SEM image of the transfer film on the ball after tribo-testing.

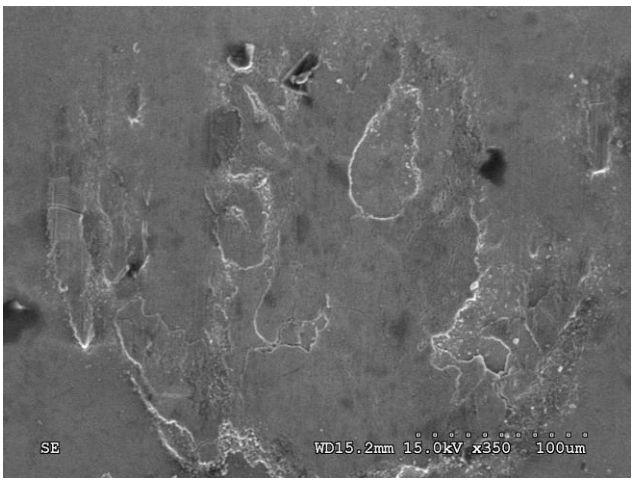

Figure 33: SEM image of ball after tribo-testing

Table 5: EDS analysis of ball after tribo-testing

Element	**At%**
C	27.37
O	26.95
Si	0.74
Cr	7.61
Mn	0.26
Fe	27.58
Mo	9.49
Total	**100**

The DLC and Mo-DLC films were also tested under oil lubrication. Mo-DLC with 2 at.% and 6 at.% Mo has shown the lowest friction coefficient compared the rest of the films. However, all COF were low with very small differences from each other. Mo-DLC with 6 at.% and 2 at.% has shown friction coefficient of 0.065 and 0.07 respectively. Whereas DLC and Mo-DLC with 16.9 at.% has shown steady state friction coefficient of 0.085 and 0.095. None of the films has shown any sign of wear even after 3000 m. The COF variation is shown in Figure 34. COF plot is very stable for all the films as well. This may be due to the fact that the particular oil used for the experiments was very viscous and did not allow significant differences between these films to be fully revealed.

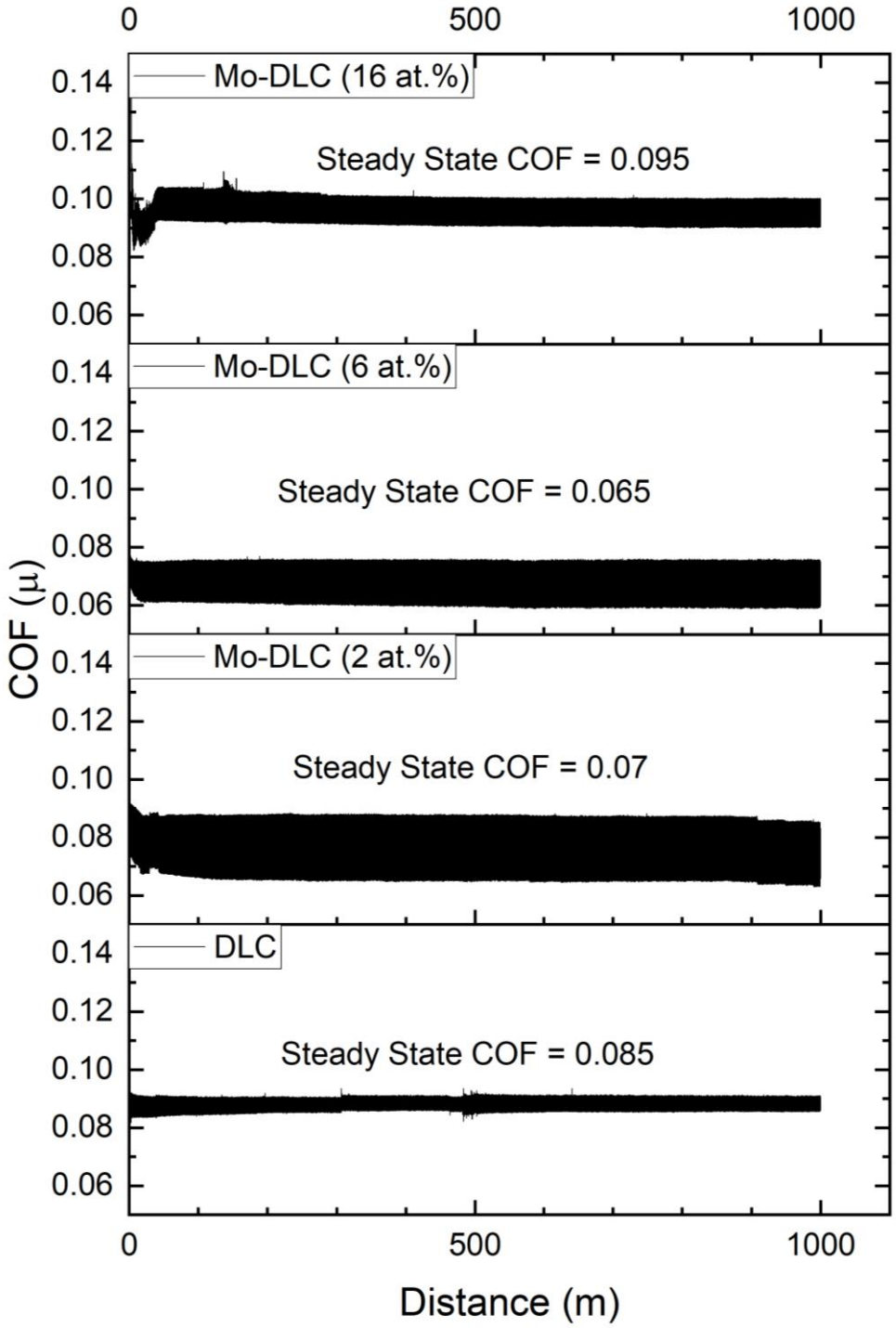

Figure 34: COF plot for films in oil lubrication condition

CHAPTER 6

CONCLUSIONS

- Good quality DLC can be deposited with pulsed DC power applied on the substrate. A repetition frequency of 60 kHz resulted in moderate power on the substrate holder and produced very smooth films with good deposition rate.
- Properties of Mo-DLC were not found to depend on the type of power supply used on substrate and target. Deposition rate is mainly affected by power supply.
- The hardness of the Mo-DLC films decreased with increasing Mo content. Incorporating more Mo in the films form, more MoC that produces a hardness increase while reducing the residual stresses.
- When Mo is introduced into the film at 4.2 at.% it starts to form cubic MoC in nanocrystalline form. These MoC nanocrystalline particles are surrounded by graphitic boundaries. The size of MoC increases with increase in Mo content. Even at 16.9 at.% Mo, there were graphitic boundaries around MoC. Which results into good mechanical and tribological properties of film.
- For both dry and oil lubrication condition, Mo-DLC with 6 at.% Mo showed excellent tribological properties with low COF and low wear rate. While Mo-DLC with 4.2 at.% Mo showed poor tribological properties in dry sliding condition which is associated with formation of debris and MoC nanoparticles in wear track during testing.
- Based on these results, further reduction in COF is possible at room temperature by using oil with active Sulphur additives.

References:

1. Chung, D.D.L., “Review Graphite”, Journal of Materials Science, 37, 1475–1489 (2002). https://doi.org/10.1023/A:1014915307738
2. Palshin, V., Meletis, E., Ves, S., & Logothetidis, S., “Characterization of ion-beam-deposited diamond-like carbon films”, Thin Solid Films, 270, 165–172 (1995) https://doi.org/10.1016/0040-6090(95)06912-7
3. Liu, Y., Erdemir, A., & Meletis, E., “An investigation of the relationship between graphitization and frictional behavior of DLC coatings”, Surface and Coatings Technology, 86, 564–568 (1996) https://doi.org/10.1016/s0257-8972(96)03057-5
4. Liu, Y., Erdemir, A., & Meletis, E., “A study of the wear mechanism of diamond-like carbon films”, Surface and Coatings Technology, 82, 48–56 (1996) https://doi.org/10.1016/0257-8972(95)02623-1
5. Meletis, E., Erdemir, A., & Fenske, G., “Tribological characteristics of DLC films and duplex plasma nitriding/DLC coating treatments”, Surface and Coatings Technology, 73, 39–45 (1995) https://doi.org/10.1016/0257-8972(94)02375-1
6. Liu, Y., & Meletis, E., “Evidence of graphitization of diamond-like carbon films during sliding wear”, Journal of Materials Science, 32, 3491–3495 (1997) https://doi.org/10.1023/a:1018641304944
7. Wang, J., Sugimura, Y., Evans, A., & Tredway, W. , “The mechanical performance of DLC films on steel substrates”, Thin Solid Films, 325(1–2), 163–174 (1998) https://doi.org/10.1016/s0040-6090(98)00418-0

8. Yu, G. Q., Lee, S. H., & Lee, J., “Effects of thermal annealing on amorphous carbon nitride films by r.f. PECVD”, Diamond and Related Materials, 11(9), 1633–1637 (2002) https://doi.org/10.1016/s0925-9635(02)00111-5
9. Tang, X., Wang, H., Feng, L., Shao, L., & Zou, C., “Mo doped DLC nanocomposite coatings with improved mechanical and blood compatibility properties”, Applied Surface Science, 311, 758–762 (2014) https://doi.org/10.1016/j.apsusc.2014.05.155
10. Constantinou, M., Pervolaraki, M., Koutsokeras, L., Prouskas, C., Patsalas, P., Kelires, P., Giapintzakis, J., & Constantinides, G., “Enhancing the nano scratch resistance of pulsed laser deposited DLC films through molybdenum-doping”, Surface and Coatings Technology, 330, 185–195 (2017) https://doi.org/10.1016/j.surfcoat.2017.09.048
11. Müller, I. C., Sharp, J., Rainforth, W. M., Hovsepian, P., & Ehiasarian, A., “Tribological response and characterization of Mo–W doped DLC coating”, Wear, 376–377, 1622–1629 (2017) https://doi.org/10.1016/j.wear.2016.11.036
12. Hovsepian, P. E., Mandal, P., Ehiasarian, A. P., Sáfrán, G., Tietema, R., & Doerwald, D., “Friction and wear behaviour of Mo–W doped carbon-based coating during boundary lubricated sliding” Applied Surface Science, 366, 260–274 (2016) https://doi.org/10.1016/j.apsusc.2016.01.007
13. Aisenberg, S., & Chabot, R., “Ion-Beam Deposition of Thin Films of Diamondlike Carbon”, Journal of Applied Physics, 42(7), 2953–2958 (1971) https://doi.org/10.1063/1.1660654
14. Oelhafen, P., Freeouf, J., Harper, J., & Cuomo, J., “Electron spectroscopy study of hydrogenated amorphous carbon films formed by methane ion beam deposition”, Thin Solid Films, 120(3), 231–238 (1994) https://doi.org/10.1016/0040-6090(84)90299-2

15. Robertson, J., “Diamond-like amorphous carbon”, Materials Science and Engineering: R: Reports, 37(4–6), 129–281 (2002) https://doi.org/10.1016/s0927-796x(02)00005-0
16. Lifshitz, Y., “Hydrogen-free amorphous carbon films: correlation between growth conditions and properties”, Diamond and Related Materials, 5(3–5), 388–400 (1996) https://doi.org/10.1016/0925-9635(95)00445-9
17. Lifshitz, Y., “Diamond-like carbon — present status”, Diamond and Related Materials, 8(8–9), 1659–1676 (1999) https://doi.org/10.1016/s0925-9635(99)00087-4
18. Voevodin, A., Donley, M., & Zabinski, J., “ Pulsed laser deposition of diamond-like carbon wear protective coatings: a review”, Surface and Coatings Technology, 92(1–2), 42–49 (1997) https://doi.org/10.1016/s0257-8972(97)00007-8
19. Siegal, M., Tallant, D., Barbour, J., Provencio, P., Martinez-Miranda, L., & DiNardo, N., “Characterization of amorphous carbon films grown by pulsed-laser deposition”, High Powered Laser Ablation (1998) https://doi.org/10.2172/658461
20. Gupta, P., Singh, V., & Meletis, E., “Tribological behavior of plasma-enhanced CVD a-C:H films. Part I: effect of processing parameters”, Tribology International, 37(11–12), 1019–1029 (2004) https://doi.org/10.1016/j.triboint.2004.07.020
21. Gupta, P., & Meletis, E., “Tribological behavior of plasma-enhanced CVD a-C:H films. Part II: multinanolayers”, Tribology International, 37(11–12), 1031–1038 (2004) https://doi.org/10.1016/j.triboint.2004.07.021
22. Li, K., & Hsu, S., “A quantitative wear measurement method on production engine parts: Effect of DLC thin films on wear” Wear, 426–427, 462–470 (2019) https://doi.org/10.1016/j.wear.2019.01.054

23. Ali, N., Kousar, Y., Okpalugo, T., Singh, V., Pease, M., Ogwu, A., Gracio, J., Titus, E., Meletis, E., & Jackson, M., "Human micro-vascular endothelial cell seeding on Cr-DLC thin films for mechanical heart valve applications", Thin Solid Films, 515(1), 59–65 (2006) https://doi.org/10.1016/j.tsf.2005.12.023
24. Robertson, J., "Deposition mechanisms for promoting sp3 bonding in diamond-like carbon", Diamond and Related Materials, 2(5–7), 984–989 (1993) https://doi.org/10.1016/0925-9635(93)90262-z
25. Jacob, W., & Möller, W., "On the structure of thin hydrocarbon films", Applied Physics Letters, 63(13), 1771–1773 (1993) https://doi.org/10.1063/1.110683
26. Erdemir, A., & Donnet, C., "Tribology of diamond-like carbon films: recent progress and prospects", Journal of Physics D: Applied Physics, 39(18), R311–R327 (2006) https://doi.org/10.1088/0022-3727/39/18/r01
27. Nir, D., "Intrinsic stress in diamond-like carbon films and its dependence on deposition parameters", Thin Solid Films, 146(1), 27–43 (1997) https://doi.org/10.1016/0040-6090(87)90337-3
28. Fallon, P., Veerasamy, V., Davis, C., Robertson, J., Amaratunga G., Milne, W., & Koskinen, J., "Properties of filtered-ion-beam-deposited diamondlike carbon as a function of ion energy", Physical Review B, 48(7), 4777–4782 (1993) https://doi.org/10.1103/physrevb.48.4777
29. McKenzie, D., Muller, D., & Pailthorpe, B., "Compressive-stress-induced formation of thin-film tetrahedral amorphous carbon", Physical Review Letters, 67(6), 773–776 (1991) https://doi.org/10.1103/physrevlett.67.773

30. Dai, M., Wei, C., Zhou, K., Zhu, M., Hou, H., Lin, S., & Tong, X., "Properties of W/DLC/W–S–C composite films fabricated by magnetron sputtering", Transactions of Nonferrous Metals Society of China, 25(9), 3002–3011 (2015) https://doi.org/10.1016/s1003-6326(15)63927-9
31. Müller, I., Sharp, J., Rainforth, W., Hovsepian, P., & Ehiasarian, A., "Tribological response and characterization of Mo–W doped DLC coating", Wear, 376–377, 1622–1629 (2017) https://doi.org/10.1016/j.wear.2016.11.036
32. Varma, A., Palshin, V., Meletis, E., & Fountzoulas, C., "Tribological behaviour of Si–DLC coatings", Surface Engineering, 15(4), 301–306 (1999) https://doi.org/10.1179/026708499101516641
33. Meng, W., Meletis, E., Rehn, L., & Baldo, P., "Inductively coupled plasma assisted deposition and mechanical properties of metal-free and Ti-containing hydrocarbon coatings" Journal of Applied Physics, 87(6), 2840–2848 (2000) https://doi.org/10.1063/1.372266
34. Varma, A., Palshin, V., & Meletis, E., "Structure–property relationship of Si-DLC films", Surface and Coatings Technology, 148(2–3), 305–314 (2001) https://doi.org/10.1016/s0257-8972(01)01350-0
35. Palshin, V., Tittsworth, R., Fountzoulas, C., & Meletis, E., "X-ray absorption spectroscopy, simulation and modeling of Si-DLC films", Journal of Materials Science, 37(8), 1535–1539 (2002) https://doi.org/10.1023/a:1014960616824
36. Wang, F., Jiang, J., & Meletis, E., "Self-assembled Co nanorods in diamond-like carbon thin films synthesized by plasma-assisted magnetron sputtering", Applied Physics Letters, 83(12), 2423–2425 (2003) https://doi.org/10.1063/1.1610813

37. Wang, F., Jiang, J., & Meletis, E., “Microstructural evolution of Co nanostructures in diamond-like carbon by plasma-assisted processing”, Journal of Applied Physics, 95(9), 5069–5074 (2004) https://doi.org/10.1063/1.1691181
38. Singh, V., Jiang, J., & Meletis, E., “Cr-diamondlike carbon nanocomposite films: Synthesis, characterization and properties”, Thin Solid Films, 489(1–2), 150–158 (2005) https://doi.org/10.1016/j.tsf.2005.04.104
39. Ali, N., Kousar, Y., Okpalugo, T., Singh, V., Pease, M., Ogwu, A., Gracio, J., Titus, E., Meletis, E., & Jackson, M., “Human micro-vascular endothelial cell seeding on Cr-DLC thin films for mechanical heart valve applications”, Thin Solid Films, 515(1), 59–65 (2006) https://doi.org/10.1016/j.tsf.2005.12.023
40. Meletis, E., & Jiang, J., “Ordered, Self-Organized Cobalt Nanodots in Co-Diamond-Like Carbon Thin Films”, Journal of Nanoscience and Nanotechnology, 6(6), 1807–1810 (2006) https://doi.org/10.1166/jnn.2006.213
41. Singh, V., Palshin, V., Tittsworth, R., & Meletis, E., “Local structure of composite Cr-containing diamond-like carbon thin films”, Carbon, 44(7), 1280–1286 (2006) https://doi.org/10.1016/j.carbon.2005.10.048
42. Pal, S., Jiang, J., & Meletis, E., “Effects of N-doping on the microstructure, mechanical and tribological behavior of Cr-DLC films”, Surface and Coatings Technology, 201(18), 7917–7923 (2007) https://doi.org/10.1016/j.surfcoat.2007.03.036
43. Jiang, J., Wang, F., & Meletis, E., “Fabrication and thermal stability of Co nanopillars in diamondlike carbon films”, International Journal of Nanomanufacturing, 2(1/2), 80 (2007) https://doi.org/10.1504/ijnm.2008.017841

44. Venkatesh, M., Taktak, S., & Meletis, E., “Synthesis of Ag-doped hydrogenated carbon thin films by a hybrid PVD–PECVD deposition process” Bulletin of Materials Science, 37(7), 1669–1676 (2014) https://doi.org/10.1007/s12034-014-0728-4
45. Venkatesh, M., Taktak, S., & Meletis, E., “Characterization of nanocomposite a-C:H/Ag thin films synthesized by a hybrid deposition process”, Physics of Metals and Metallography, 116(8), 825–834 (2015) https://doi.org/10.7868/s0015323015080173
46. Tang, X., Wang, H., Feng, L., Shao, L., & Zou, C., “Mo doped DLC nanocomposite coatings with improved mechanical and blood compatibility properties”, Applied Surface Science, 311, 758–762 (2014) https://doi.org/10.1016/j.apsusc.2014.05.155
47. Constantinou, M., Pervolaraki, M., Koutsokeras, L., Prouskas, C., Patsalas, P., Kelires, P., Giapintzakis, J., & Constantinides, G., “Enhancing the nanoscratch resistance of pulsed laser deposited DLC films through molybdenum-doping”, Surface and Coatings Technology, 330, 185–195 (2017) https://doi.org/10.1016/j.surfcoat.2017.09.048
48. Padmanaban, D., Mohan, L., Giri, P., Bera, P., Anandan, C., & Barshilia, H., “Effect of Molybdenum Content on Mechanical and Tribological Properties of Diamond-Like Carbon Coatings over Titanium β-21S Alloy”, C 7(1) (2021) https://doi.org/10.3390/c7010001
49. Sánchez-López J.C., Fernández A., “Doping and Alloying Effects on DLC Coatings. In: Donnet C., Erdemir A. (eds)”, Tribology of Diamond-Like Carbon Films, Springer (2008) https://doi.org/10.1007/978-0-387-49891-1_12
50. Chang, Y., Wang, D., & Wu, W., “Catalysis effect of metal doping on wear properties of diamond-like carbon films deposited by a cathodic-arc activated deposition process”, Thin Solid Films, 420–421, 241–247 (2002) https://doi.org/10.1016/s0040-6090(02)00801-5

51. Corbella, C., “Preparation of metal (W, Mo, Nb, Ti) containing a-C:H films by reactive magnetron sputtering”, Surface and Coatings Technology. (2003) https://doi.org/10.1016/s0257-8972(03)01025-9
52. S. Gunjan, Fabrication and characterization of cobalt-diamond-like carbon nano composites, The University of Texas at Arlington, 2007
53. Ji, L., Li, H., Zhao, F., Chen, J., & Zhou, H., “Microstructure and mechanical properties of Mo/DLC nanocomposite films” Diamond and Related Materials, 17(11), 1949–1954 2008 https://doi.org/10.1016/j.diamond.2008.04.018
54. Koidl P., Wild C., Locher R., Sah R., “Amorphous, Hydrogenated Carbon Films and Related Materials: Plasma Deposition and Film Properties. In: Clausing R.E., Horton L.L., Angus J.C., Koidl P. (eds)”, Diamond and Diamond-like Films and Coatings. NATO ASI Series (Series B: Physics), vol 266. Springer, Boston, MA, (1991) https://doi.org/10.1007/978-1-4684-5967-8_12
55. Liu, Y., Erdemir, A., & Meletis, E., “Influence of environmental parameters on the frictional behavior of DLC coatings” Surface and Coatings Technology, 94–95, 463–468 (1997) https://doi.org/10.1016/s0257-8972(97)00450-7
56. Erdemir, A., Eryilmaz, O., Nilufer, I., & Fenske, G., “Effect of source gas chemistry on tribological performance of diamond-like carbon films”, Diamond and Related Materials 93-96, 632–637 (2000) https://doi.org/10.1016/s0925-9635(99)00361-1
57. Erdemir, A., Eryilmaz, O., & Fenske, G., “Synthesis of diamondlike carbon films with superlow friction and wear properties” Journal of Vacuum Science & Technology A: Vacuum, Surfaces, and Films, 18(4) 1987–1992 (2000) https://doi.org/10.1116/1.582459

58. Dimigen, H., & Klages, C. P., “Microstructure and wear behavior of metal-containing diamond-like coatings”, Surface and Coatings Technology, 49(1–3), 543–547 (1991) https://doi.org/10.1016/0257-8972(91)90114-c
59. Hip Science | Science Mission Directorate. (2002). NASA. https://science.nasa.gov/science-news/science-at-nasa/2002/30oct_hipscience
60. Krishna, K., Umeno, M., Nukaya, Y., Soga, T., & Jimbo, T., “Photovoltaic and spectral photoresponse characteristics of n-C/p-C solar cell on a p-silicon substrate”, Applied Physics Letters, 77(10), 1472–1474 (2002) https://doi.org/10.1063/1.1290687